Electronics Research Laboratory
University of California
Berkeley, California

MICROWAVE SCATTER FROM A ROUGH WATER SURFACE

by

G. O. Hendry
R. H. Clarke

This research was supported by the Fir Force Office of Scientific Research of the Office of Aerospace Research; the Department of the Army, Army Research Office; and the Department of the Navy, Office of Naval Research, under Grant No. AF-AFOSR-139-63.

June 7, 1963

ACKNOWLEDGMENT

The authors wish to thank Mr. Fred Clapp, Mr. Ernie Rasmussen, and Mr. Norm Tanner for their valuable help in the design and construction of the experimental apparatus.

ABSTRACT

This report presents both theoretical and experimental investigations into the problem of the reflection of electromagnetic radiation obliquely incident on a surface of random profile.

The theory indicates that the signal received in the specular direction can be considered to consist of a constant signal, together with a non-Rayleigh random signal. The constant signal has the same phase as that received if the surface were smooth, but is reduced in magnitude by the roughness. The random signal consists of two independent components in phase quadrature; the variance of the component in phase with the constant signal is in general smaller than that in phase quadrature with it, and the magnitudes of these variances are found to depend on the area of rough surface illuminated as well as on the roughness itself.

Experimental confirmation of these theoretical results has been obtained, using a rippled-water surface whose roughness could be accurately controlled and measured.

TABLE OF CONTENTS

		Page
Section I.	INTRODUCTION	1
Section II.	A THEORY OF SCATTERING FROM A ROUGH SURFACE	2
II. 1	Electromagnetic Basis	3
II. 2	Scatterers Composed of Many Surface Variations	9
II. 3	Scaterers Composed of Few Surface Variations	10
II. 4	Time-Average Power	23
II. 5	Summary of Theory	24
Section III.	APPARATUS AND APPROXIMATIONS	26
III. 1	The Spherical Wave Approximation	26
III. 2	The Gently Sloping Surface Approximation	29
III. 3	The Infinitely-Conducting-Scatterer Approximation	33
III. 4	Summary of Approximations	35
Section IV.	SURFACE MEASUREMENTS	36
IV. 1	The Probability Density of Surface Height	36
IV. 2	The Surface Autocorrelation Function	41
Section V.	MEASUREMENT OF SPECULAR SCATTER	49
V. 1	Measurement of Time-Average Power	49
V. 2	Measurement of s_r^2 Relative to s_i^2	57
V. 3	Summary of Electromagnetic Measurements	63
Section VI.	CONCLUSION	64
Section VII.	APPENDIX	66
VII. 1	Calculation of $\rho_{rx}(\xi)$	66
VII. 2	Calculation of $\rho_{ix}(\xi)$	70
Section VIII.	REFERENCES	73

LIST OF FIGURES

FIGURE		PAGE
1	Plane Wave Incident on Rough Scatterer.	4
2	Surface Element Illuminated by Plane Wave Passing Through Grid Element x, y.	4
3	Plane Wave Source with Direction of Electric Field Indicated (⟶)	7
4	A Sample of Length a of a Random Quantity z . . .	13
5	A Sample of Length b of the Random Quantity $Av\left\{z(x)_y\right\}_a$	13
6	A vs. a/ξ_o	15
7	Dependence on x of z, ψ, $\sin\psi$, and $\cos\psi$.	20
8-a	S_i^2 and S_r^2 vs. $\psi_o \frac{a}{\xi_{ox}} = \frac{b}{\xi_{oy}} = 1$	21
8-b	S_i^2 and S_r^2 vs. $\psi_o \frac{a}{\xi_{ox}} = \frac{b}{\xi_{oy}} = 2$	21
8-c	S_r^2 and S_i^2 vs. $\psi \frac{a}{\xi_{ox}} = \frac{b}{\xi_{oy}} = 5$	22
8-d	The Maximum Value of $S_r^2 + S_i^2$ as a Function of Sample Size	22
9	Relationship Between E, E_r, E_r', and E_i.	25
10	Ripple Tank.	27
11	Spherical Wave Diffraction from S to p^1	30
12	Relationship Between the Plane Wave Source Axis, z', and the Specular Direction	31
13-a	Dependence of the Magnitude of the Reflection Coefficient on the Angle of Incidence.	34
13-b	Dependence of the Angle of the Reflection Coefficient on the Angle of Incidence.	34
14	Schematic of Analog Used to Measure $\rho(\varepsilon)$.	38

LIST OF FIGURES

FIGURE		PAGE
15	Comparison Between $\rho(\ )$ Experimental and $\rho(\varepsilon) = \frac{1}{\sqrt{2\pi}\,1.45}\int_{\varepsilon}^{\infty} \exp\left\{\frac{-z^2}{2(1.45)^2}\right\} dz$ for Roughness V	40
16-a	Analog for Measuring $\rho(\xi)$	42
16-b	Probe Carriage	43
16-c	Bridge Schematic	44
16-d	Detector Schematic	44
17-a	Autocorrelation Function $\rho_x(\xi)$ for Roughness V	47
17-b	Autocorrelation Function $\rho_y(\xi)$ for Roughness V	47
18	Circuit Used for Measuring Time Average Power	50
19	Normalized Power vs. Standard Deviation of Phase for 30 inch Parabola	52
20	Normalized Power vs. Standard Deviation of Phase for the 10 inch Parabola	52
21-a	$S_i^2 + S_r^2$ Experimental (10 inch Parabola)	53
21-b	$S_i^2 + S_r^2$ Theoretical $(\frac{a}{\xi_{ox}} = \frac{b}{\xi_{oy}} = 2)$	53
22	Microwave Bridge Used to Measure E_r' and E_i	59
23	Phasor Diagram Illustrating the Relationship Between the Field Components at the Crystal	60
24	Circuit Used to Measure $E_r'^2$ and E_i^2	61
25-a	S_i^2 and S_r^2 Experimental (10 inch Parabola)	62
25-b	S_i^2 and S_r^2 Theoretical $(\frac{a}{\xi_{ox}} = \frac{b}{\xi_{oy}} = 2)$	62

I. INTRODUCTION

The general behavior of scatter from a rough-water surface has been known for some time.[1] Recent measurements, however, have left a good deal to be explained about some aspects of this problem.[2] In particular, it has been noted that actual measurements of scattered field depart from theory when the surface is very rough.

This report presents a theory that appears to predict the behavior of specular scatter from a rough surface. This theory is tested by actual scattering measurements from experimental rough-water surfaces whose roughness could be accurately controlled and measured. Good agreement with theory is obtained.

The theoretical development is carried out in Section II. The experimental apparatus and surface measurements are discussed in Sections III and IV. The microwave scattering measurements are presented in Section V.

II. A THEORY OF SCATTERING FROM A ROUGH SURFACE

The problem of scattering from a rough surface is complicated by the fact that the exact surface detail is not usually known. As a result of this difficulty, several approximate solutions have been proposed. Ament[3] followed the direct approach of applying Maxwell's equations to the statistical boundary but was unable to evaluate the resulting integrals. Another approach[4] has been to consider the rough reflecting surface as a phase-changing diffracting screen and so obtain the angular power spectrum of the scattered radiation. The approach to the problem presented in this section is based on Huygens' principle. A Huygens source is associated with each element on the surface, and the scattered field is considered to be the summation of contributions from these sources. The advantage of this approach is that the field rather than the energy is found, and, hence the detailed phase information is not lost.

The analysis will first be developed in terms of a static rough scatterer and expressions for the field scattered in the specular direction derived.* These expressions cannot be evaluated unless the exact detail of the rough scatterer is known. They may, however, be closely approximated if the scatterer is composed of many surface variations. If the surface detail of the scatterer is allowed to become time-variant, the scattered signal varies in a statistical manner. The relationship between the statistical behavior of this time-variant signal and the statistical description of the surface will be derived.

The approach developed in this section will be limited to the specular direction and will assume a gently sloping surface with radius of curvature very much greater than the electromag-

* The specular direction is the direction of a ray optically reflected from the scatterer if the scatter were a smooth plane surface.

netic wave length λ. The results of this analysis are useful not only in explaining subsequent experimental results but also seem to apply to scattering measurements made over the ocean.

II.1 Electromagnetic Basis

Consider a plane wave incident at an angle θ_o on the static perfectly-conducting rectangular rough scatterer lying in the x-y plane illustrated in Fig. 1. The electric field e_x is perpendicular to the plane of incidence. The plane wave passes through an imaginary flat grid of infinitesimal rectangular elements which lie just above the rough scatterer. The dimensions of each of the grid elements is dx by dy. Since the radius of curvature of the surface is very much greater than the electromagnetic wave length λ, the element of plane wave passing through grid element x, y is optically reflected by the surface at point x, y, z. Since the surface has also been assumed to be perfectly conducting, the energy passing through element x, y of the grid is all reflected into a new plane wave whose direction is given by Snell's law and the slope of the surface at point x, y. This scattering process is illustrated in Fig. 2.

Considering now the combined effect of all the elemental plane waves incident on the surface, it is possible to specify the field just above the surface in terms of the elemental reflected plane waves. The equivalence principle[5] states that if this field is replaced by equivalent electric and magnetic currents, the scattered field may be found in terms of the equivalent currents in the absence of the conducting boundary. This is particularly useful for the case at hand because of the complicated boundary conditions. The simplification lies in the fact that the boundary need be considered only in the determination of the fields just above the boundary. The effect of the boundary on the radiation produced by these fields is eliminated.

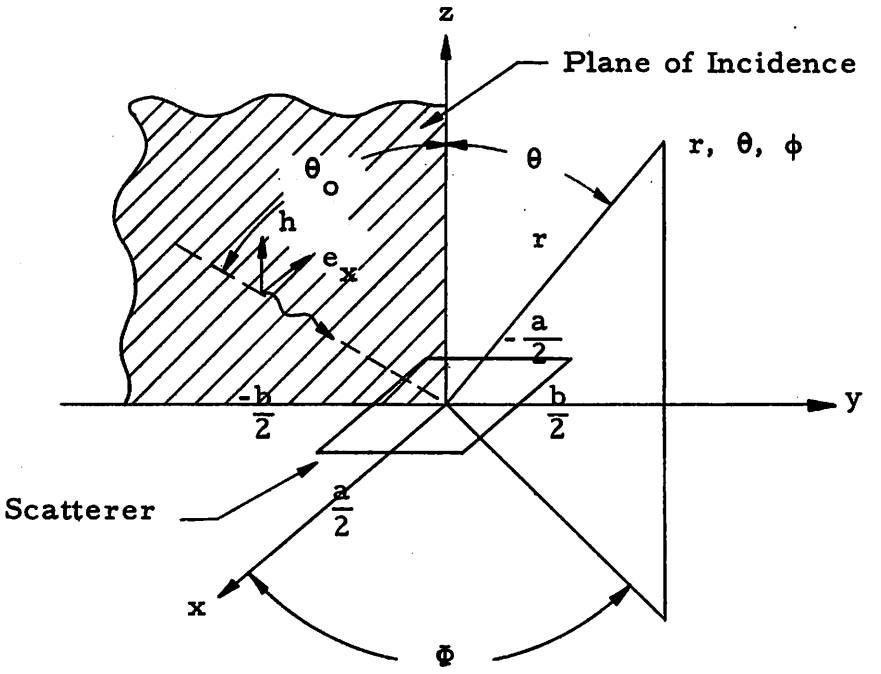

Fig. 1 Plane Wave Incident on Rough Scatterer

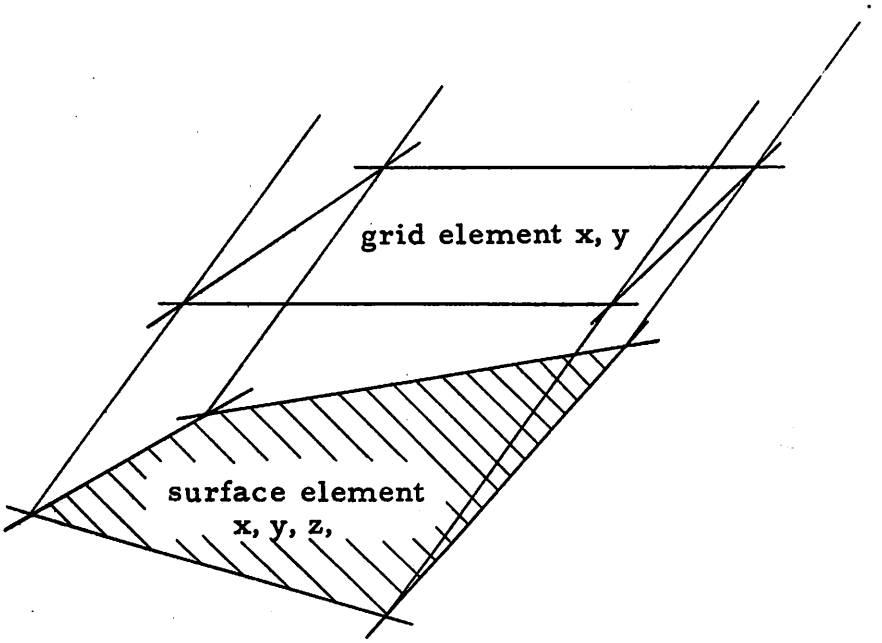

Fig. 2 Surface Element Illuminated by Plane Wave Passing Through Grid Element x, y.

The problem now is to find the equivalent currents just above the surface and the radiation field produced by these currents. Consider again the elemental plane wave which passes through the grid element x, y and is scattered from the surface at point x, y, z. Since the elemental reflected wave is plane in the vicinity of x, y, z it may be replaced by an elemental plane-wave source consisting of the equivalent electric and magnetic currents discussed above.[6] This plane-wave source is just a Huygens source of the type that contains both electric and magnetic current. The electric field pattern of a rectangular plane wave source is given by

$$e_\theta' = \frac{je_x'}{\lambda} \frac{\exp(-jkr')}{r'} \cos^2\left(\frac{\theta'}{2}\right) \cos(\phi')\, dx'\, dy'$$

$$e_\phi' = \frac{-je_x'}{\lambda} \frac{\exp(-jkr')}{r'} \cos^2\left(\frac{\theta'}{2}\right) \sin(\phi')\, dx'\, dy'$$

where the primed co-ordinates refer to the plane of the Huygens source which is the plane normal to the direction of travel of the reflected plane wave and which includes the point x, y, z on the surface of the scatterer. The above equations refer to a rectangular plane-wave source as illustrated in Fig. 3. Due to the sloping surface the actual plane-wave sources are not, in general, rectangular, and their dimensions vary. This can be taken into account by considering that the power passing through the rectangular grid element at point x, y must be conserved. Thus by representing $e_x'\, dx'\, dy'$ in the above expressions by $e_x \sqrt{\cos\theta_o'}\, dx\, dy$, we insure the conservation of power without influencing the directional properties of the Huygens source. The Huygens source located at point x, y, z on the surface thus has an electric field given by

$$e_\theta' = \frac{je_x \exp(-jkr')}{\lambda \quad r'} \cos^2\left(\frac{\theta'}{2}\right) \cos(\phi') \sqrt{\cos\theta_o}\, dx\, dy \qquad (1\text{-a})$$

$$e_{\phi}' = \frac{-je_x \exp(-jkr')}{\lambda \quad r'} \cos^2 \frac{\theta'}{2} \sin(\phi') \cos \theta_o \, dx \, dy \qquad (1\text{-b})$$

The plane wave incident on the rough scatterer has its electric field polarized in the x direction. The perfectly-conducting boundary requires that e_y on the boundary be 0, regardless of the slope of the surface; this in turn requires that e_x', the total electric field in the scattered plane wave, have no y component. This requirement, along with the requirement that z' lies along the direction of travel of the reflected plane wave and the requirement that the origin of the primed system lie at point x, y, z, is sufficient to establish the relationship between x, y, z and x', y'z'.

The field scattered from the static rough scatterer may now be found by Huygens principle by summing the field contributions from the Huygens sources on the surface. In order to obtain a solution to this problem let us restrict ourselves to the case of far-zone specular scatter. Since the angle of incidence of the plane wave is θ_o at $\phi = -\pi/2$, the specular direction will be θ_o at $\phi = +\pi/2$. The fact that the specular point of observation is in the far zone of the scatterer implies that if the scatterer were smooth the field contributions from the sources on the scatterer would all be in phase. Since the scatterer is not smooth, the phase Ψ of the contribution from the source at point x, y, z on the surface of the scatterer is advanced by $2kC_o z$, where, $C_o = \cos \theta_o$ and

$$k = \frac{2\pi}{\lambda}$$

is the propagation constant of free space. If the surface is gently sloping it is possible to assume that $\theta' - \theta_o \approx 0$.* Thus by Eqs. (1) the amplitude and polarization of the contributions from the sources

---

* The effect of this approximation is discussed in Section III.

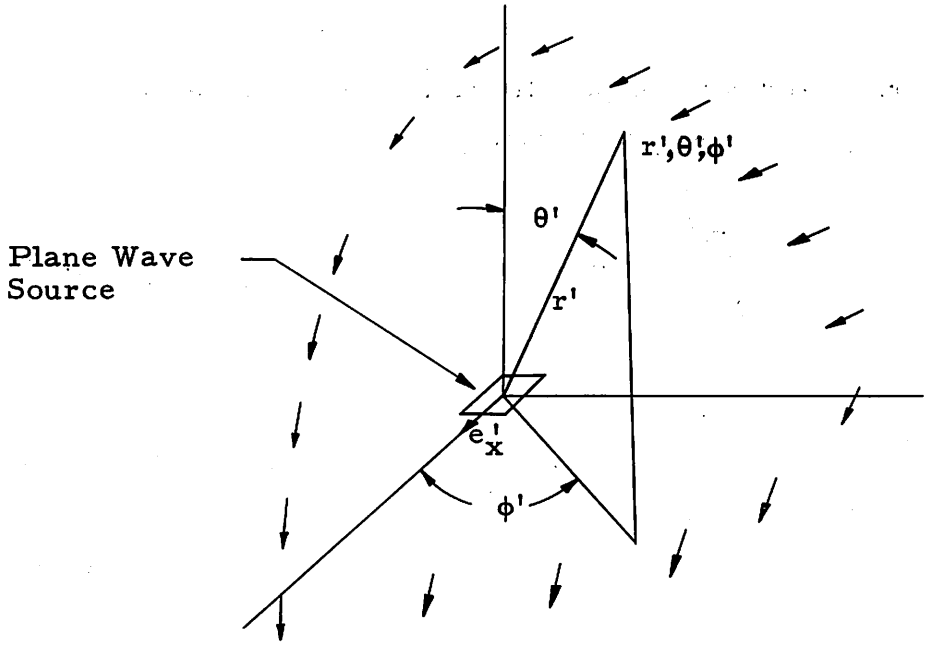

Fig. 3 Plane Wave Source with Direction of Electric Field Indicated (⟶)

on the scatterer are approximately constant. The contribution of a single elemental Huygens source located at point x, y, z on the rough scatterer to the far-zone specular field is then approximately

$$de \approx \frac{e_x}{\lambda r'} \exp\ (\ + j2kC_o z\ (x, y))\ \sqrt{C_o}\ dx\ dy$$

where now only the phase of the contribution, $2kC_o z\ (x, y)$, is a function of position on the scatterer. The total field is just the integral over the imaginary grid of these elemental contributions. The total normalized far-zone specular field from a gently sloping rectangular rough scatterer whose dimensions are a by b is thus approximately

$$E = \frac{1}{ab} \int_{-a/2}^{a/2} \int_{-b/2}^{b/2} \exp\ (j2kC_o z\ (x, y))\ dx\ dy$$

where E is normalized with respect to the smooth surface field. Substituting $\Psi(x, y)$ for $2kC_o z(x, y)$, obtain

$$E = \frac{1}{ab} \int_{-a/2}^{a/2} \int_{-b/2}^{b/2} \exp\left(j\Psi(x, y)\right) dx\, dy = E_r + jE_i \qquad (2\text{-a})$$

$$E_r = \frac{1}{ab} \int_{-a/2}^{a/2} \int_{-b/2}^{b/2} \cos\left(\Psi(x, y)\right) dx\, dy = \mathrm{Av}\left\{\cos\left(\Psi(x, y)\right)\right\}_{ab} \qquad (2\text{-b})$$

$$E_i = \frac{1}{ab} \int_{-a/2}^{a/2} \int_{-b/2}^{b/2} \sin\left(\Psi(x, y)\right) dx\, dy = \mathrm{Av}\left\{\sin\left(\Psi(x, y)\right)\right\}_{ab} \qquad (2\text{-c})$$

where $\mathrm{Av}\left\{\ \right\}_{ab}$ denotes the average over the scatterer.

Equations (2) predict the far-zone specular scatter from a gently-sloping rough scatterer whose surface detail is static. If the surface detail of the scatterer is time-variant, Eqs. (2) predict the scattered field at one instant of time. *

To evaluate Eqs. (2) the exact surface detail must be known. Rough surfaces, however, are generally described statistically. Thus, while it is not possible to evaluate E_r and E_i exactly, it is possible to predict their statistical behavior. The remainder of this section will be devoted to evaluating Eqs. (2) in terms of the statistical description of the surface.

---

*Time-variant rough surfaces also produce a Dopler frequency shift on the scattered signal. This effect is small, however, if the frequency of the surface variations is very much less than the electromagnetic frequency

II. 2. Scatterers Composed of Many Surface Variations

In order to evaluate Eqs. (2) it is necessary to know the exact detail of the rough scattering surface. Rough surfaces, however, are seldom specified exactly but are usually described in statistical terms. In this section an approximate relationship between the probability density of surface height and the scattered field will be considered.

If the surface has many variations about its mean value, the portion of the surface lying in the range dz about z is given very nearly but not exactly by

$$ab\ p(z)\ dz$$

where ab is the area of the x-y plane containing the scatterer and p(z) is the probability density of surface height of a population of surface variations of which the scatterer is a large sample. Since the experimental surfaces to be studied (Section IV) have approximately Gaussian distributions of surface height, p(z) will be assumed Gaussian

$$p(z) = \frac{1}{\sqrt{2\pi}\,\sigma} \exp\left\{-\frac{z^2}{2\sigma^2}\right\}$$

where σ is the standard deviation of surface height. Since the phase of a contribution to the far-zone specular field is linearly related ($\Psi(x, y) = 2kC_o z(x, y)$) to the height of the element making the contribution, the distribution of phase of the far-zone specular field contributions will also be Gaussian. Defining $p(\Psi)$ as the probability density of the phase of the far-zone specular field contributions, obtain

$$p(\Psi) = \frac{1}{\sqrt{2\pi}\,\Psi_o} \exp\left\{-\frac{\Psi^2}{2\Psi_o^2}\right\} \qquad (3\text{-a})$$

$$\Psi_o = 2kC_o\sigma \qquad (3\text{-b})$$

where Ψ_o is the standard deviation of phase.

The portion of surface making field contributions whose phases lie in the range $d\Psi$ about Ψ is given very nearly but not exactly by

$$ab\ p(\Psi)\ d\Psi$$

It is thus possible to approximate the integrals of Eqs. (2) by averaging over phase instead of over the surface.

$$E_r = Av\left\{\cos\left(\Psi(x,y)\right)\right\}_{ab} \approx \frac{1}{ab}\int_{-\infty}^{\infty} ab\ p(\Psi)\cos(\Psi)\,d\Psi = \exp\left\{-\frac{\Psi_o^2}{2}\right\} \quad (4\text{-a})$$

$$E_i = Av\left\{\sin\left(\Psi(x,y)\right)\right\}_{ab} \approx \frac{1}{ab}\int_{-\infty}^{\infty} ab\ p(\Psi)\sin(\Psi)\,d\Psi = 0 \quad (4\text{-b})$$

This result was derived by Pekeris and independently by McFarlane during World War II.[3]

The approximation lies in the fact that the Gaussian distribution of surface height assumed is true only for an infinite sample of surface variations. Since a finite scatterer represents at best a large sample of this population, the distribution of height of such a scatterer is not exactly Gaussian. As the scatterer represents an increasingly large sample of the roughness population, the approximations represented by Eqs. (4) are improved. A quantitative relationship between the sample size and the error in these approximations is developed in the next section.

II. 3 Scatterers Composed of Few Surface Variations

If the scatterer is composed of only a few variations about its mean value, the assumption that the height distribution of the

scatterer is Gaussian is not valid. This is true because the scatterer now only represents a small sample of the roughness population. Eqs. (4), therefore, are not a good approximation to the scattered field. The error in Eqs. (4) is a statistical function of the size of the scatterer, the surface height distribution, and the surface autocorrelation function.*

So far the surface detail of the scatterer has been considered time-invariant. Let us now consider time-variant rough surfaces and concentrate first on the average of E_r and E_i with respect to time. Averaging E_r over time is equivalent to averaging E_r over many different samples of the population of surface variations. The time average of E_r is thus determined by a large sample of the roughness population. Eq. (4-a) then applies, and the time average of E_r must approach $\exp\left\{-\frac{\psi_o^2}{2}\right\}$ as the averaging time is increased. A similar argument shows that the time average of E_i must approach 0.

Eqs. (3) still apply to the instantaneous field of the time-variant rough scatterer. Defining E_r' as $E_r - \exp\left\{-\frac{\psi_o^2}{2}\right\}$ and applying Eqs. (2), obtain

---

*The surface autocorrelation function which is discussed more fully in Section IV is defined

$$\rho(\xi) = \lim \frac{\int_{-R}^{R} z(r)z(r+\xi)\,dr}{\int_{-R}^{R} z(r)^2\,dr}$$

The autocorrelation function of a surface rough in two dimensions has two components $\rho_x(\xi)$ and $\rho_y(\xi)$ which refer to the surface correlation in the x and y directions, respectively. These functions are expressed in terms of ξ_{ox} and ξ_{oy}, where ξ_{ox} and ξ_{oy} may be thought of qualitatively as the average roughness width in the x and y directions, respectively. Common forms assumed for the autocorrelation function are $\exp\left\{-\frac{\xi^2}{\xi_o^2}\right\}$ and $\exp\left\{-\left|\frac{\xi}{\xi_o}\right|\right\}$. It is evident that if $\xi = \xi_o$, the correlation given by either of these forms is 1/e.

$$E = \exp\left\{-\frac{\Psi_o^2}{2}\right\} + E_r' + jE_i \tag{5-a}$$

$$E_r' = \mathrm{Av}\left\{\cos\left(\Psi(xy)\right) - \exp\left\{-\frac{\Psi_o^2}{2}\right\}\right\}_{ab} \tag{5-b}$$

$$E_i = \mathrm{Av}\left\{\sin\left(\Psi(xy)\right)\right\}_{ab} \tag{5-c}$$

E_r' is a statistical function of time with a time-average value of zero and a variance (standard deviation squared) of s_r^2 about zero. E_i is also a statistical function of time having a time-average value of zero and a variance of s_i^2 about zero. s_r^2 and s_i^2 may also be thought of as the standard deviations of the error to be expected in Eqs. (4). The problem is now to relate s_i^2 and s_r^2 to the size and the statistical description of the scatterer.

Consider an instantaneous profile of a random quantity z which is a function of a single variable x. This is illustrated in Fig. 4. It may be shown[4] that the instantaneous average of z over a sample of length a, $\mathrm{Av}\left\{z(x)\right\}_a$, has a variance s^2 about the time average of z given by

$$s^2 = VA \tag{6-a}$$

$$V = \int_{-\infty}^{\infty} z^2 p(z)dz \tag{6-b}$$

$$A = 2\int_0^1 (1-u)\,\rho_x(ua)du \tag{6-c}$$

where V is the variance of z about its time average, p(z) is the probability density of z, and $\rho_x(\xi)$ is the autocorrelation function of z. A is called the "sampling parameter."

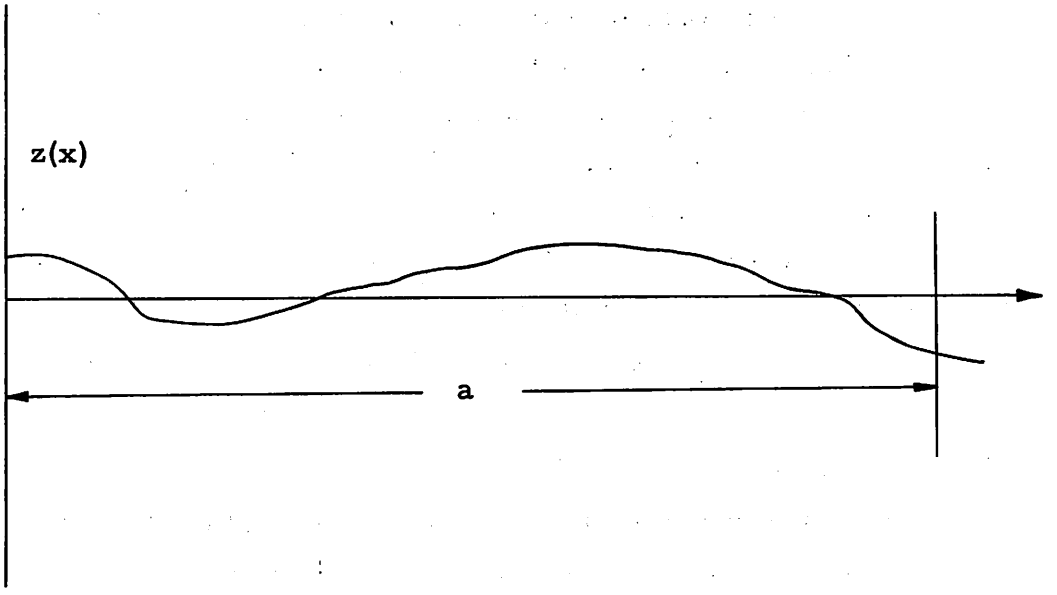

Fig. 4 A sample of Length a of a Random Quantity z

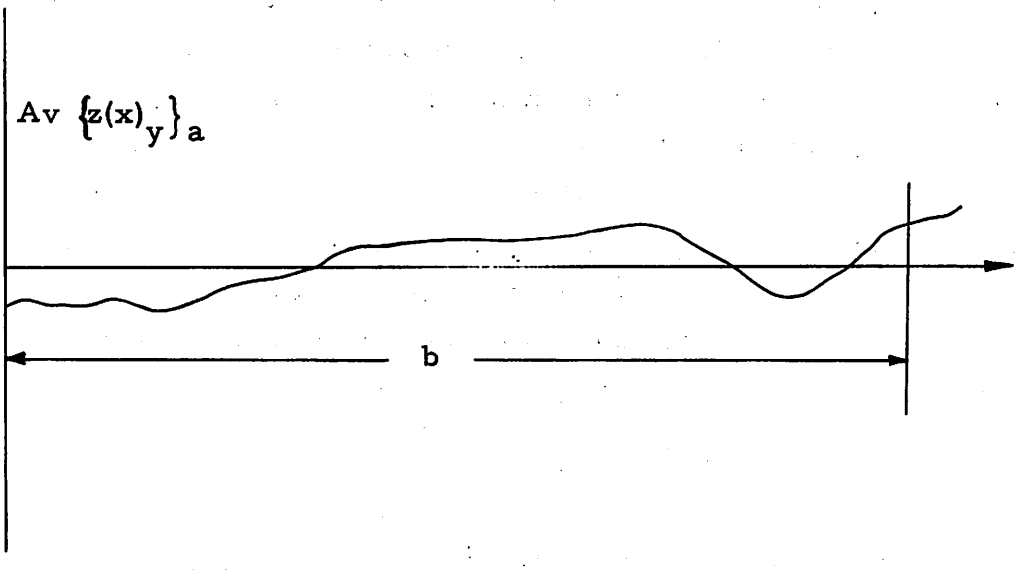

Fig. 5 A Sample of Length b of the Random Quantity Av $\{z(x)_y\}_a$

The significance of A may be inferred from Fig. 6, which shows the dependence of A on the sample length $\underline{a}$ divided by the correlation distance ξ_o. a/ξ_o ~~small implies that the average is~~ being taken over only a small part of one variation of z. This corresponds to an A of unity which implies that $\mathrm{Av}\left\{z(x)\right\}_a$ has a variance equal to the variance of z. a/ξ_o large implies that the average is being taken over many variations of z. For this case A becomes small and hence s^2 becomes small. Thus A is seen to relate the variance of $\mathrm{Av}\left\{z(x)\right\}_a$ to the sample size a/ξ_o.

Examination of Fig. 6 indicates that A is not very dependent on the form of the autocorrelation function $\rho(\xi)$ as long as $\rho(\xi)$ is monotonically decreasing. This fact is useful when it is necessary to approximate the A resulting from a complicated autocorrelation function. Thus if one can find ξ_o for the complicated autocorrelation function, $\rho(\xi)$ may be approximated by $\exp\left\{-\left|\frac{\xi}{\xi_o}\right|\right\}$ and an approximate value of A obtained.

In the case of the random scatterer, z is a random function of two variables and therefore Eq. (5) cannot be applied directly. The case previously considered will thus be extended to the case of two variables. The scatterer may be thought of as a rectangular sample of the surface variation population having a length $\underline{a}$ in the x-direction and a length b in the y direction. Divide this sample into strips of length $\underline{a}$ and width dy. The instantaneous average of z over the strip at y is defined as $\mathrm{Av}\left\{z(x)_y\right\}_a$ (the average of z(x)at y over a). Fig. 5 shows this strip average as a function of y. Clearly the instantaneous average of z over the whole sample, $\mathrm{Av}\left\{z\ (x, y)\right\}_{ab}$, is the average of $\mathrm{Av}\left\{z(x)_y\right\}_a$ over a sample of length b in the y direction.

$$\mathrm{Av}\left\{z(x, y)\right\}_{ab} = \mathrm{Av}\left\{\mathrm{Av}\left\{z(x)_y\right\}_a\right\}_b$$

$z(x)_y$ is a function of only one variable x. Eqs. (6) therefore apply and $\mathrm{Av}\left\{z(x)_y\right\}_a$ has a variance s_x^2 of

$$s_x^2 = VA_x$$

$$V = \int_{-\infty}^{+\infty} z^2\, p(z)\, dz$$

$$A_x = 2\int_0^1 (1-u)\ \rho_x(ua)\, du$$

where $\rho_x(\xi)$ denotes the autocorrelation function of z with respect to x. The autocorrelation function of $\mathrm{Av}\left\{z(x)_y\right\}_a$ with respect to y is the same as the autocorrelation function of z with respect to y, $\rho_y(\xi)$. $\mathrm{Av}\left\{z(x)_y\right\}_a$ is therefore a function of a single

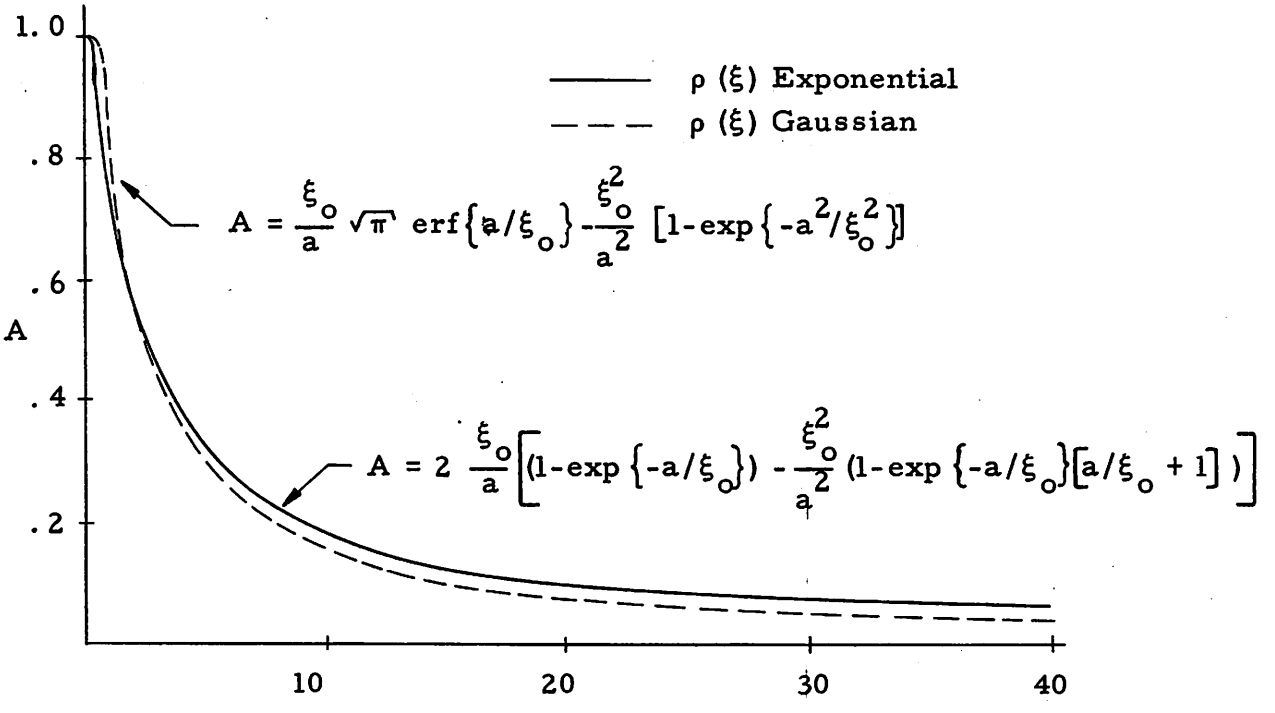

Fig. 6 A vs. a/ξ_o

variable y having a variance VA_x and an autocorrelation function $\rho_y(\xi)$. Eqs. (6) may now be applied to determine the variance s of $Av\left\{z(x,y)\right\}_{ab}$. The result is:

$$s^2 = VA_xA_y \tag{7-a}$$

$$V = \int_{-\infty}^{+\infty} z^2 p(z)dz \tag{7-b}$$

$$A_x = 2\int_0^1 (1-u)\,\rho_x(ua)\,du \tag{7-c}$$

$$A_y = 2\int_0^1 (1-u)\,\rho_y(ub)du \tag{7-d}$$

s^2 defined by Eqs. (7) gives the variance of the instantaneous average of a random function of two variables about the time average of the function. While this may be thought of physically as the variance of the instantaneous average of surface height, the result applies to any random function of two variables. Consider the application of Eqs. (7) to Eq. (5-b). $\cos(\Psi(x,y)) - \exp\left\{-\frac{\Psi_o^2}{2}\right\}$ now replaces z and E_r' given by $Av\left\{\cos(\Psi(x,y)) - \exp\left\{-\frac{\Psi_o^2}{2}\right\}\right\}_{ab}$ replaces $Av\left\{z(x,y)\right\}_{ab}$. Defining V_r as the variance of $\cos(\Psi(x,y)) - \exp\left\{-\frac{\Psi_o^2}{2}\right\}$ and ρ_{rx} and ρ_{ry} as the autocorrelation functions of $\cos(\Psi(x,y)) - \exp\left\{-\frac{\Psi_o^2}{2}\right\}$, the variance s_r^2 of E_r' is given by:

$$s_r^2 = V_rA_{rx}A_{ry} \tag{8-a}$$

$$V_r = \int_{-\infty}^{+\infty} \left[\cos(\Psi) - \exp\left\{-\frac{\Psi_o^2}{2}\right\}\right]^2 p(\Psi)\, d\Psi \qquad (8\text{-b})$$

$$A_{rx} = 2\int_0^1 (1-u)\,\rho_{rx}(ua)\,du \qquad (8\text{-c})$$

$$A_{ry} = 2\int_0^1 (1-u)\,\rho_{ry}(ub)\,du \qquad (8\text{-d})$$

$$\rho_{rx}(\xi) = \lim_{x\to\infty} \frac{\int_{-x}^{x}\left[\cos(\Psi(x,y)) - \exp\left\{-\frac{\Psi_o^2}{2}\right\}\right]\left[\cos(\Psi(x+\xi,y)) - \exp\left\{-\frac{\Psi_o^2}{2}\right\}\right]dx}{\int_{-x}^{x}\left[\cos(\Psi(x,y)) - \exp\left\{\left(-\frac{\Psi_o^2}{2}\right)\right\}\right]^2 dx} \qquad (8\text{-e})$$

$$\rho_{ry}(\xi) = \lim_{y\to\infty} \frac{\int_{-y}^{y}\left[\cos(\Psi(x,y)) - \exp\left\{-\frac{\Psi_o^2}{2}\right\}\right]\left[\cos(\Psi(x,y+\xi)) - \exp\left\{-\frac{\Psi_o^2}{2}\right\}\right]dy}{\int_{-y}^{y}\left[\cos(\Psi(x,y)) - \exp\left(-\frac{\Psi_o^2}{2}\right)\right]^2 dy} \qquad (8\text{-f})$$

A similar argument shows that E_i has a variance s_i^2 about its time average of zero given by

$$s_i^2 = V_i A_{ix} A_{iy} \qquad (9\text{-a})$$

$$V_i = \int_{-\infty}^{+\infty} \sin^2(\Psi)\, p(\Psi)\, d\Psi \qquad (9\text{-b})$$

$$A_{ix} = 2\int_0^1 (1-u)\,\rho_{ix}(ua)\,du \qquad (9\text{-c})$$

$$A_{iy} = 2 \int_0^1 (1 - u)\, \rho_{iy}(ub)\, du \qquad (9\text{-d})$$

$$\rho_{ix} = \lim_{x \to \infty} \frac{\int_{-x}^{x} \sin(\Psi(x, y)) \sin(\Psi(x + \xi, y)\, dx}{\int_{-x}^{x} \sin^2(\Psi(x, y))\, dx} \qquad (9\text{-e})$$

$$\rho_{iy} = \lim_{y \to \infty} \frac{\int_{-y}^{y} \sin(\Psi(x, y)) \sin(\Psi(x, y + \xi)\, dy}{\int_{-y}^{y} \sin^2(\Psi(x, y))\, dy} \qquad (9\text{-f})$$

By assuming the Gaussian form of $p(\Psi)$ Eq. (3), V_r and V_i become

$$V_r = \frac{1}{2}\left[1 - \exp\left\{-\Psi_o^2\right\}\right]^2$$

$$V_i = \frac{1}{2}\left[1 - \exp\left\{-2\,\Psi_o^2\right\}\right]$$

Evaluating ρ_{rx}, ρ_{ry}, ρ_{ix}, and ρ_{iy} is not as straightforward. They can be evaluated, however, by noting that the proportion in which $\Psi(x)$ and $\Psi(x+\xi)$ occur is given by the joint probability distribution of surface height. The derivation is carried out in Appendices VII. 1 and VII. 2. The results are

$$\rho_{rx}(\xi) = \frac{2 \exp\left\{-\Psi_o^2\right\}\left[\cosh\left\{\Psi_o^2\, \rho_x(\xi)\right\} - 1\right]}{\left[1 - \exp\left\{-\Psi_o^2\right\}\right]^2} \qquad (10\text{-a})$$

$$\rho_{ry}(\xi) = \frac{2 \exp\left\{-\Psi_o^2\right\}\left[\cosh\left\{\Psi_o^2\, \rho_y(\xi)\right\} - 1\right]}{\left[1 - \exp\left\{-\Psi_o^2\right\}\right]^2} \qquad (10\text{-b})$$

$$\rho_{ix}(\xi) = \frac{2 \exp\left\{-\Psi_o^2\right\} \sinh\left\{\Psi_o^2 \rho_x(\xi)\right\}}{\left[1 - \exp\left\{-2\Psi_o^2\right\}\right]} \qquad (10\text{-c})$$

$$\rho_{iy}(\xi) = \frac{2 \exp\left\{-\Psi_o^2\right\} \sinh\left\{\Psi_o^2 \rho_y(\xi)\right\}}{\left[1 - \exp\left\{-2\Psi_o^2\right\}\right]} \qquad (10\text{-d})$$

Ψ_o is the standard deviation of phase; ρ_x is the surface autocorrelation function in the x direction, and ρ_y is the surface autocorrelation function in the y direction.

Several observations concerning these functions are in order. In the first place, they all decrease monotonically from 1 and approach but do not reach zero. The rate at which they fall off depends on both Ψ_o and $\rho(\xi)$. This behavior may be qualitatively explained by Fig. 7, which illustrates the relationship between z(x), $\Psi(x)$, cos ($\Psi(x)$) and sin ($\Psi(x)$). Since z(x) and $\Psi(x)$ are linearly related, they have the same autocorrelation function $\rho(\xi)$. Sin ($\Psi(x)$) and cos ($\Psi(x)$), however, always lie in the range +1 to -1 and therefore tend to assume additional "wrinkles" as Ψ_o increases. This qualitatively explains why their autocorrelation functions fall off faster than $\rho(\xi)$. For Ψ_o small, sin $\Psi \approx \Psi$, therefore $\rho_i(\xi)$ must approach $\rho(\xi)$, which is indeed the case in Eqs. (10-c and -d). Since the mean value of cos (Ψ) is close to 1 when Ψ_o is small, it tends to have twice as many "wrinkles" as $\Psi(x)$. $\rho_r(\xi)$ should thus fall off faster than $\rho_i(\xi)$. As Ψ_o approaches zero Eqs. (10-a and -b) show that $\rho_r(\xi)$ approaches $\rho^2(\xi)$ which indeed falls off faster than $\rho_i(\xi)$.

Now that $\rho_{rx}(\xi)$, $\rho_{ry}(\xi)$, $\rho_{ix}(\xi)$, $\rho_{iy}(\xi)$, V_i and V_r are known, it is possible to evaluate s_i^2 and s_r^2 using Eqs. (8) and (9). Figure 8 represents the dependence of s_i^2 and s_r^2 on ξ_o and Ψ_o for a

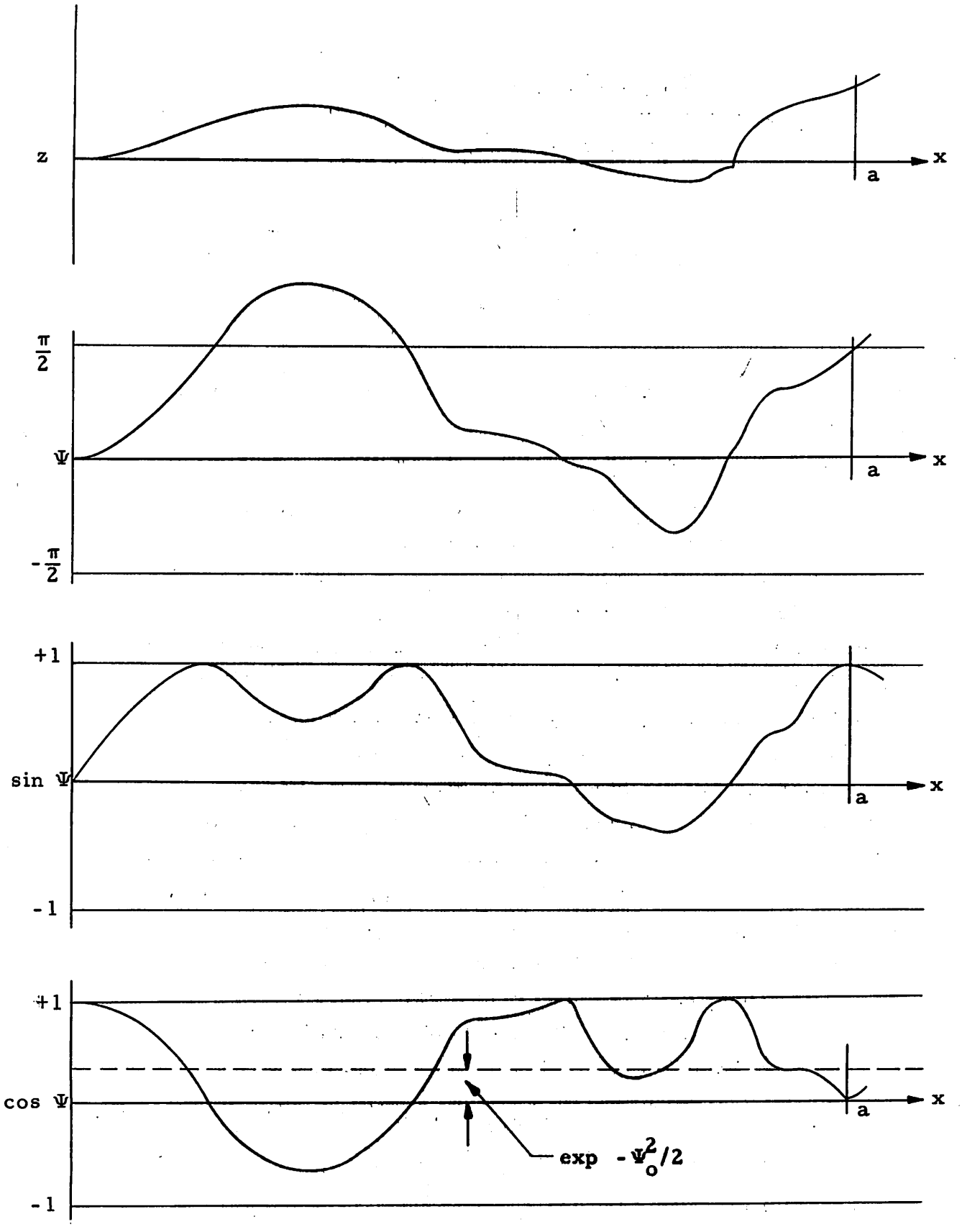

Fig. 7 Dependence on x of z, Ψ, sin Ψ, and cos Ψ

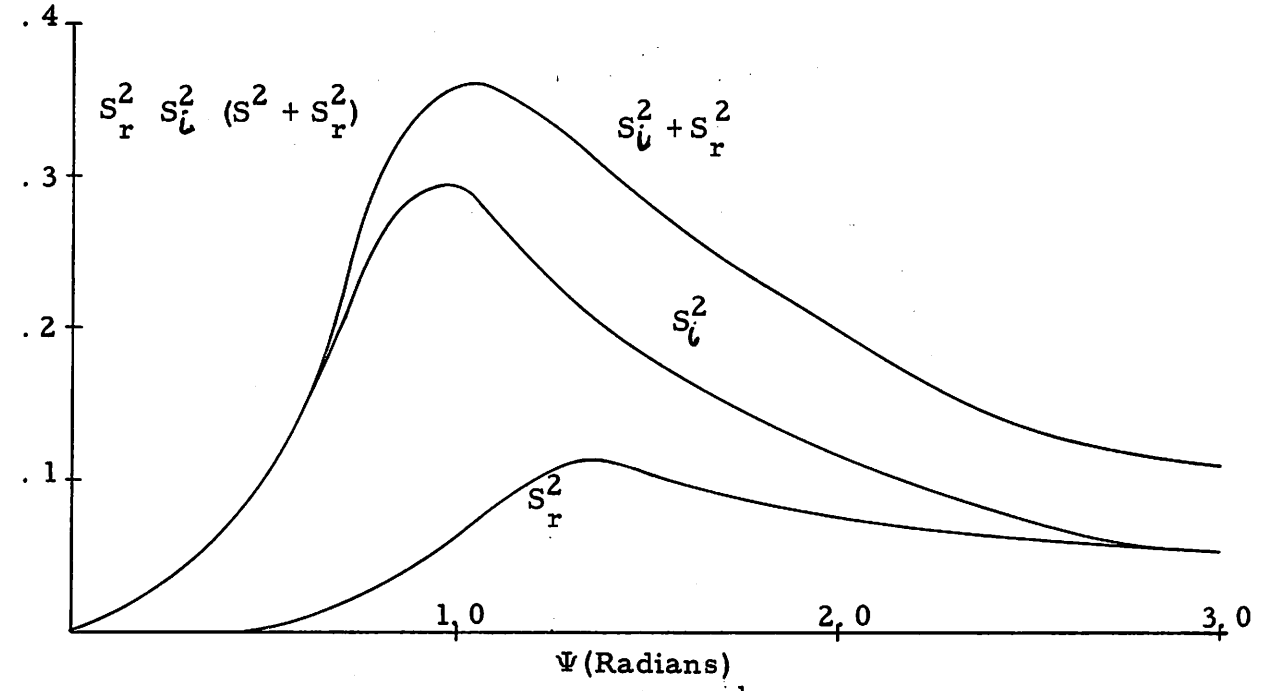

Fig. 8-a S_i^2 and S_r^2 vs. $\Psi_o \frac{a}{\xi}_{ox} = \frac{b}{\xi}_{oy} = 1$

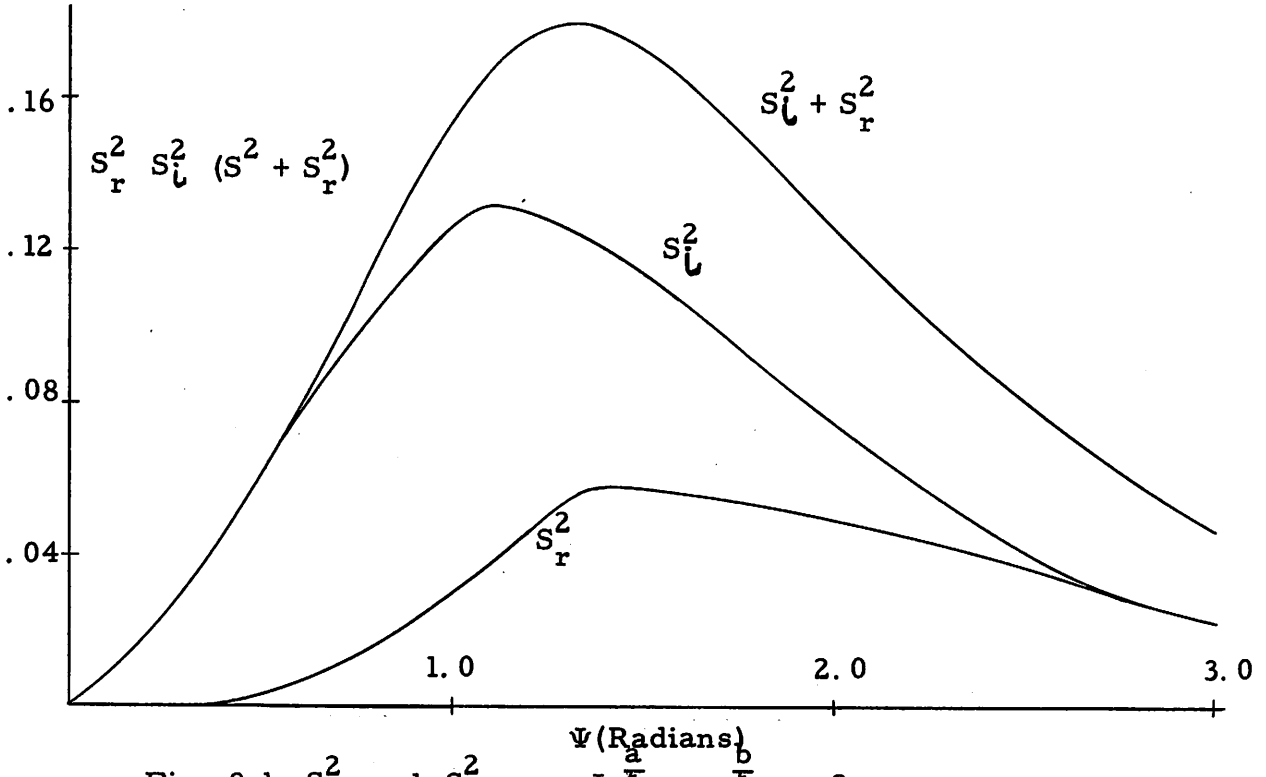

Fig. 8-b S_i^2 and S_r^2 vs. $\Psi_o \frac{a}{\xi}_{ox} = \frac{b}{\xi}_{oy} = 2$

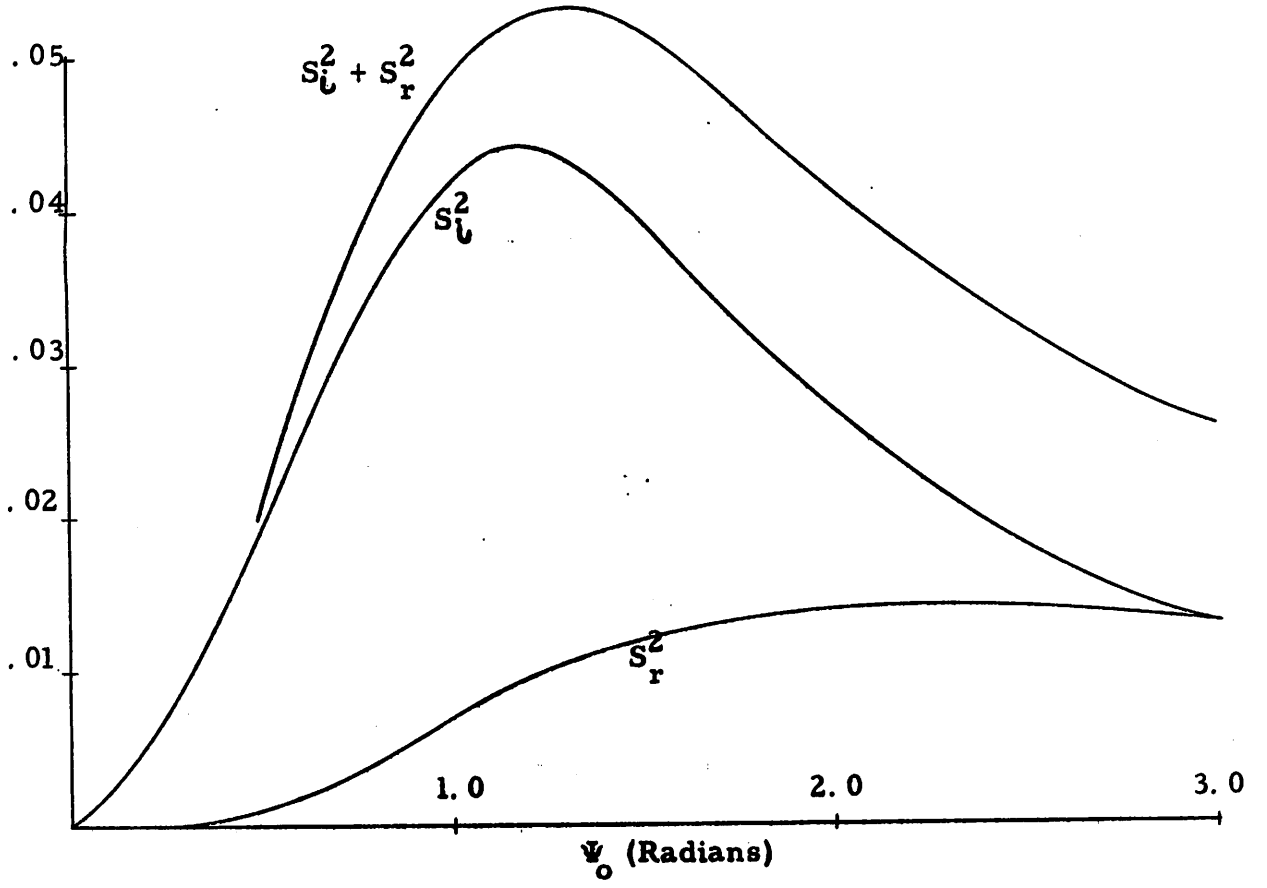

Fig. 8-C S_r^2 and S_i^2 vs. $\Psi_o \frac{a}{\xi_{ox}} = \frac{b}{\xi_{oy}} = 5$

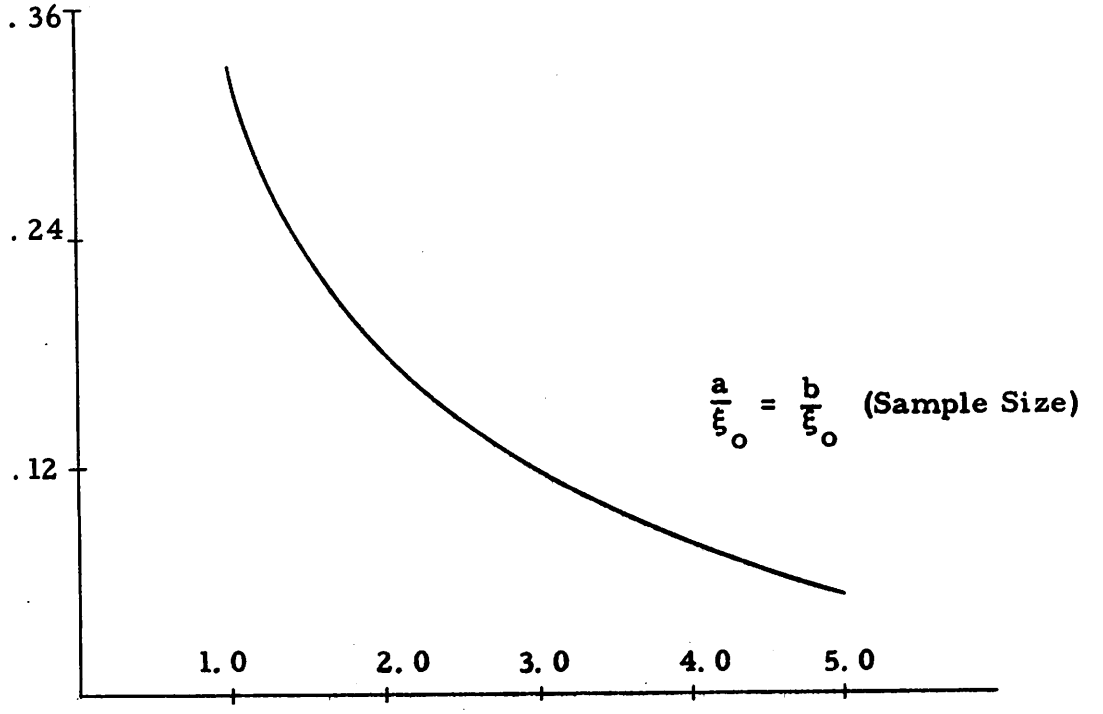

Fig. 8-D The Maximum Value of $S_r^2 + S_i^2$ as a Function of Sample Size

rectangular rough scatterer whose dimensions are a by b. These plots are constructed for the case of $a/\xi_{ox} = b/\xi_{oy}$ and for autocorrelation functions of the form $\exp\{-|\xi/\xi_o|\}$. The effect of increasing the sample size (a/ξ_{ox} by b/ξ_{oy}) is evident from these plots; as the sample size is increased both s_r^2 and s_i^2 are reduced. The behavior of s_i^2 and s_r^2 with increasing Ψ_o is of interest. s_i^2 and s_r^2 are observed to assume their maximum values for Ψ_o in the neighborhood of 1 radian. This effect was observed by Beard[2] in microwave scattering measurements made over the ocean.

II. 4 Time-Average Power

The time-average power in the specular direction is now easily related to Ψ_o, s_i^2 and s_r^2. The modulus of the total instantaneous electric field E Eq. (5-a) is

$$E^2 = \left(\exp\left\{-\frac{\Psi_o^2}{2}\right\} + E_r'\right)^2 + E_i^2$$

The normalized time average power P_{ta} is defined as

$$P_{ta} = \frac{1}{P_o} \lim_{T\to\infty} \frac{1}{T} \int_o^T P(t)\, dt$$

where P(t) is the instantaneous power and P_o is the power that would be received if the scatterer were smooth. P_{ta} is, of course, 1 if the surface is smooth.

$$P_{ta} = \lim_{T\to\infty} \int_o^T E^2\, dt = \lim_{T\to\infty} \frac{1}{T}\left[\int_o^T \exp\left\{-\Psi_o^2\right\} dt + \int_o^T 2E_r' \exp\left\{-\frac{\Psi_o^2}{2}\right\} dt + \int_o^T E_r'^2\, dt + \int_o^T E_i^2\, dt\right]$$

The second term on the right-hand side of this expression integrates to zero because E_r' is evenly distributed about zero. The third and fourth terms are just definitions of s_r^2 and s_i^2, respectively. Thus,

$$P_{ta} = \exp\left(-\Psi_o^2\right) + s_r^2 + s_i^2 \qquad (11)$$

Evidently, the time average power scattered from a rough scatterer does not depend on Ψ_o alone but also on s_r^2 and s_i^2. For scatterers containing few surface variations s_r^2 and s_i^2 will in fact dominate for Ψ_o large. This seems to be the case in measurements made of microwave scatter from the ocean.[2]

II. 5 Summary of Theory

Let us now consider the overall picture of far-zone specular scatter from a time-variant rough scatterer. It has been shown that the specular far-zone field has two-phase quadrature components E_r and E_i. E_r has a time-average or coherent component of $\exp(-\frac{\Psi_o}{2})$ with respect to the smooth surface scattered field; E_r also has a statistical component E_r' which has a variance of s_r^2. E_i has a time average of zero and a variance of s_i^2. Thus the normalized instantaneous field E is

$$E = \exp\left(-\frac{\Psi_o^2}{2}\right) + E_r' + jE_i \qquad (5\text{-a})$$

This is illustrated in Fig. 9.

s_r^2 and s_i^2 were found to depend on the size and on the statistical description of the scatterer. Increasing the number of surface variations of which the scatterer is composed reduces both s_r^2 and s_i^2; thus, the field scattered from scatterers composed of many surface variations is very nearly $\exp\left(-\frac{\Psi_o^2}{2}\right)$. The dependence of s_r^2 and s_i^2 on the standard deviation of phase, Ψ_o, produced by the rough surface, is of particular interest. s_r^2 and s_i^2 increase from zero with increasing surface roughness and reach a peak in the neighborhood of Ψ_o equal to 1 radian. Further increase in Ψ_o causes s_r^2 and s_i^2 to decrease. s_r^2 is less than s_i^2 for Ψ_o less than three radians; thus the random vector $E_r' + jE_i$ is non-Rayleigh for Ψ_o less than 3 radians.

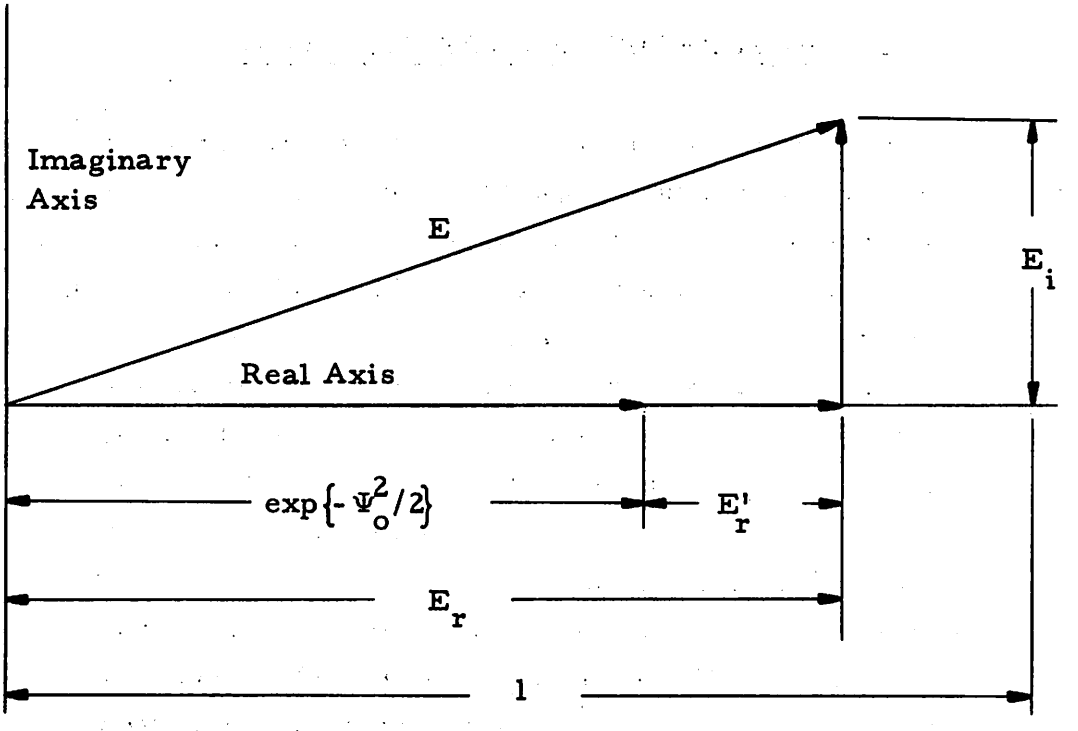

Fig. 9 Relationship between E, E_r, E'_r, and E_i.

The time-average power in the specular direction was found to be

$$P_{ta} = \exp\left(-\Psi_o^2\right) + s_r^2 + s_i^2 \qquad (11)$$

Agreement between the theory developed above and measurements of microwave scatter from the ocean was observed.

III. APPARATUS AND APPROXIMATIONS

In order to measure the rough surface scatter predicted in Section II, the experimental apparatus shown in Fig. 10 was constructed. This arrangement consists of a water surface which is roughened by a blower system. Twelve different surface roughness states were produced by controling the air intake to the blowers and the roughness parameters of each of these states measured. The rough surface is illuminated by 8-millimeter microwaves reflected from a parabolic reflector. The feed of this reflector is adjusted to produce an optical focus at the receiver when the surface is smooth. The receiver is merely an open end of wave-guide connected to a crystal detector. This apparatus is an approximation to the model analyzed in Section II. The validity of this approximation is the subject of this section.

III. 1 The Spherical Wave Approximation

Ideally, the surface would be illuminated by a plane wave and the scatter observed in the far zone of the surface. This situation is not practical in the laboratory because the surface would have to be very close to or far from the radiating structure in order to receive plane-wave illumination. Moreover, the receiver would have to be far from the surface. Yet an arrangement which causes every element of a smooth surface to produce a field contribution at the receiver which is in phase with the field contributions from all the other surface elements is an approximation to the model of Section I.

Consider a spherical wave S (Fig. 11) which is converging to point P. The field at P is just the sum of the contributions from a Huygens source distribution on S. Because of the spherical geometry the contributions at P are all of equal amplitude and phase. If a perfectly conducting infinite surface S' is now inserted between P and S, the scattered field may be determined from a Huygens source distribution on S'.

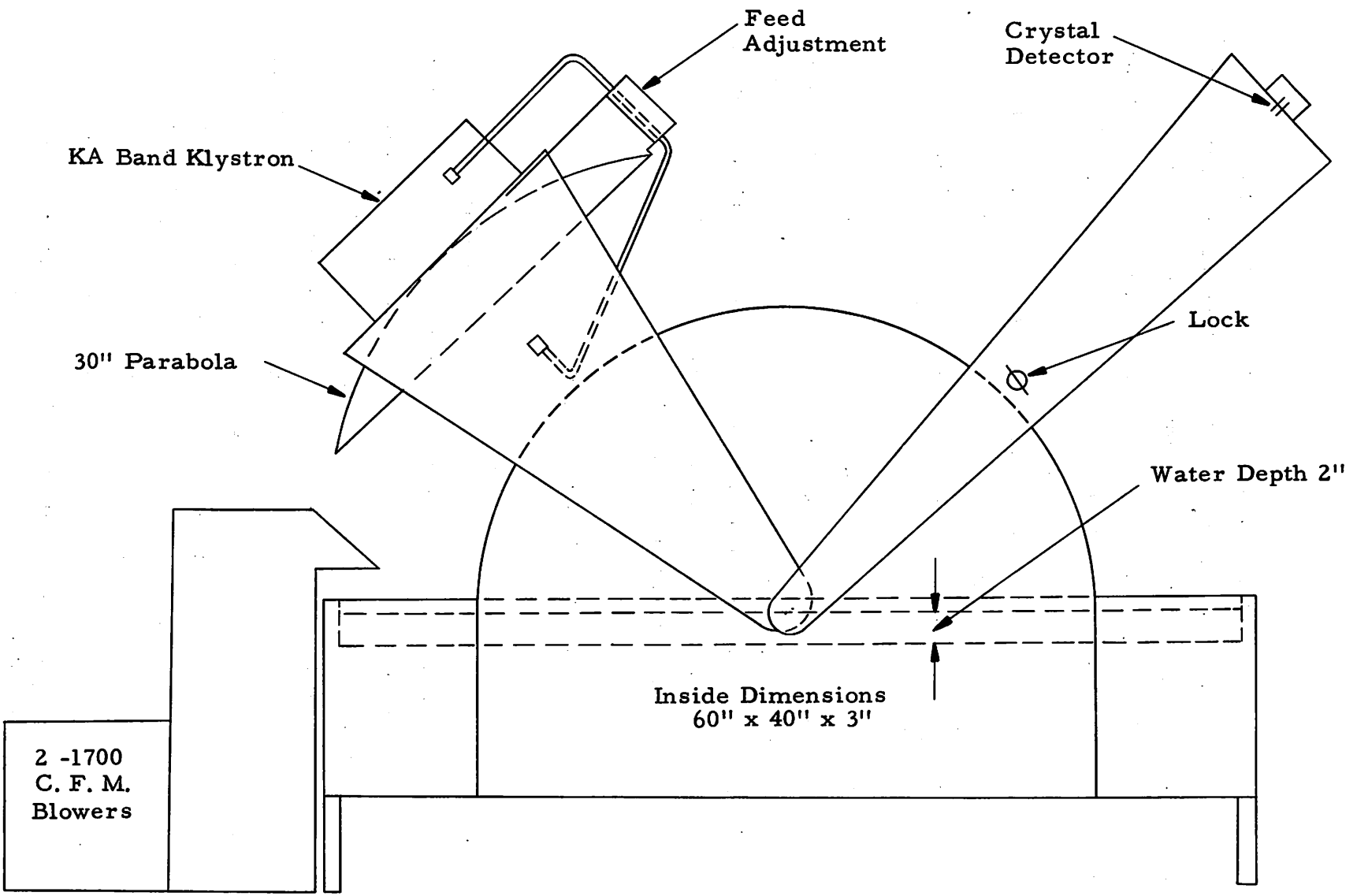

Fig. 10 Ripple Tank

The fields scattered by any element x on S' is simply a summation of plane waves. Each of these plane waves corresponds to a Huygens source on S. If the radius of curvature of S' is always sufficiently greater than λ, the surface element x reflects each of the plane waves incident upon it in accordance with Snell's law. Thus a smooth surface S' would cause the sperical wave S to converge to P' in exactly the same way that it converged to P in the absence of S'. It now remains to be shown that when S' is smooth the contributions to the field at P' from the Huygens source distribution on S' are equal in phase.

From the geometry of the problem of Fig. 11 it is evident that the shortest path between S and P' via the scattering element x is that followed by the specular plane wave a-x-P'. Other plane waves scattered via x follow paths such as b-x-P' which are longer that a-x-P' by a varying amount δ. Analytically, the field at P' due to the arbitrary scattering element x is

$$E_{P'x} = \int_S g(\theta_1)\, g(\theta_o - \theta_2)\, \exp(jk\delta)\, ds$$

where $g(\theta)$ Eq. (1) is simply the field pattern of a plane wave source. θ_o, θ_1, and θ_2 are defined by Fig 11. In the limit of zero wave length the stationary phase argument applies to the above equation and the phase of the field contribution at P' produced by element x is just the phase of the specular plane wave which follows path a-x-P'. As a varies over S, x varies over S' in such a way that the path a-x-P' remains constant. Thus each element of the smooth surface S' produces a field contribution of equal phase at P'. Therefore, in the limit of zero wave length, P' is in a certain sense in the far zone of S'. For the experimental arrangement used, θ_1 and $\theta_o - \theta_2$ never exceed 50^o while δ takes on values up to 12λ. The zero wavelength assumption would therefore seem valid to a first order approximation.

The spherical wave S' is approximated by adjusting the feed of the parabolic reflector. While only an elliptical reflector can produce a truly spherical wave, the approximation obtained using a parabola is quite good. Adjusting the parabola feed produced a very sharp focus at the receiver, thus indicating that the field contributions from the various parts of the surface are very nearly of equal phase.

The amplitude of the surface illumination is, of course, not uniform because the surface is close to the parabolic reflector. The nonuniform surface illumination will not, however, materially affect the argument leading to the approximate field equations (Eqs. 4) for scatterers composed of many surface variations. The reason for this is that Eqs. (4) depend only on the assumption that the phase of the field contributions at the receiver be normally distributed. This will be true regardless of the uniformity of the surface illumination, provided a sufficient number of surface variations are illuminated.

The predictions of Section II regarding the magnitude of the variances s_r^2 and s_i^2 (Eqs. 8 and 9) require definite knowledge of the surface illumination. In obtaining analytical expressions for these quantities, the simplest form of illumination was assumed, namely, that of uniform illumination of a rectangular rough scatterer. The complexity of the resulting expressions discourages analysis of the case at hand. The form of the Ψ_o dependence of the variances s_r^2 and s_i^2 (Figs. 8) is, however, fairly independent of the sample size. This form does not depend on uniform surface illumination and can therefore be checked with the experimental apparatus discussed above.

III. 2 The Gently Sloping Surface Approximation

In Section I the surface was assumed to be gently sloping, which made it possible to assume that the radiation patterns of the individual plane-wave sources were all aligned in the specular

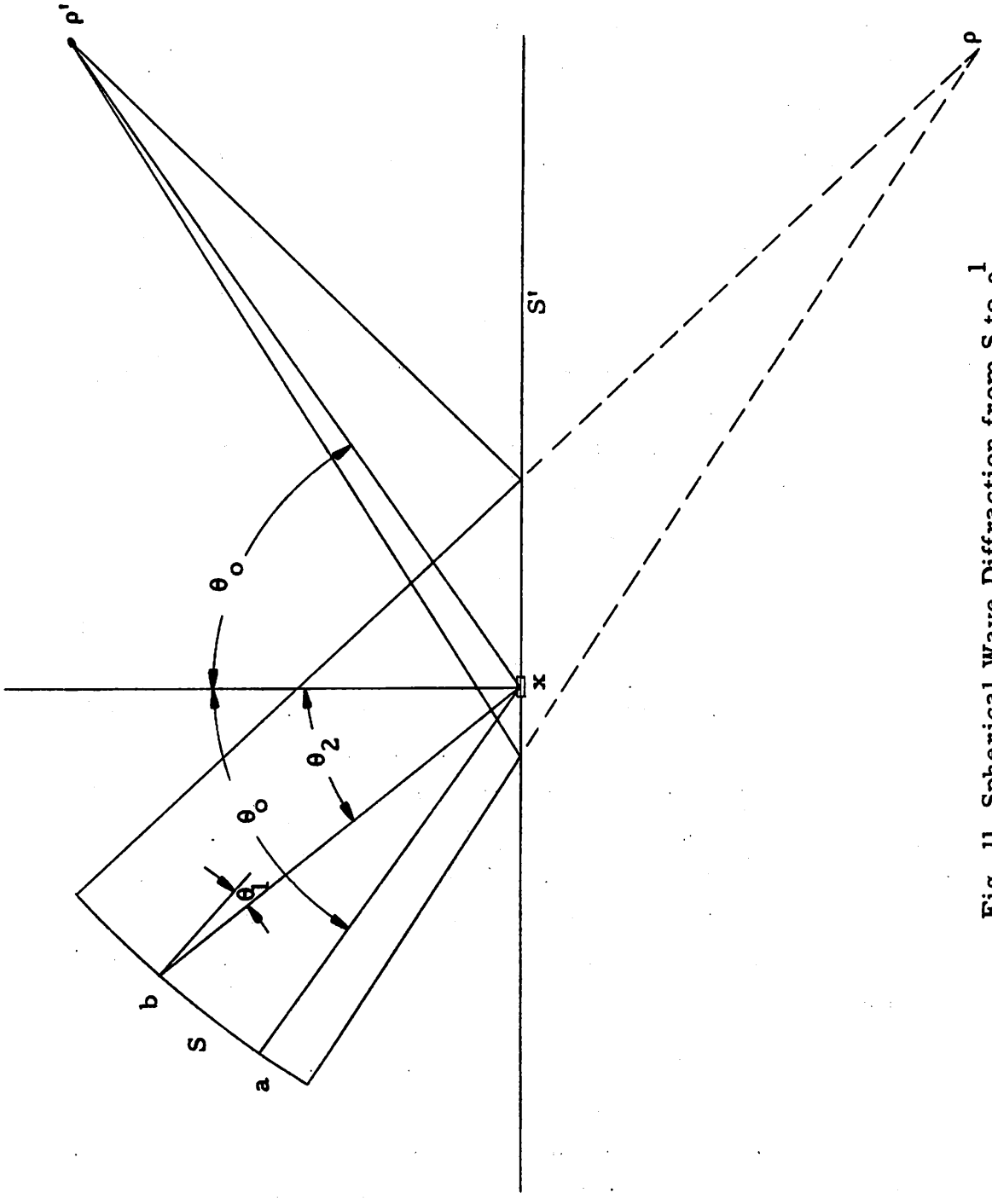

Fig. 11 Spherical Wave Diffraction from S to ρ^1

direction. If the surface is not gently sloping, the radiation patterns will be substantially misaligned with a subsequent reduction of field. It is therefore necessary to determine the effect of surface slope on the radiation pattern alignment.

Consider a surface rough only in the x-direction (uniform in the y-direction), and define the angle that any element of this surface makes with the x-y plane as δ. Since a plane wave incident on an element is reflected in accordance with Snell's law, its direction varies from the specular direction by 2δ (Fig 12). Since the radiation pattern of the elemental plane-wave source has its axis z' in the direction of the reflected plane wave, the axis of the radiation pattern is also shifted by 2δ.

If the scattering surface represents a large sample of the surface-variation population, the portion of surface having angles in the range $d\delta$ about δ is given by dS, where

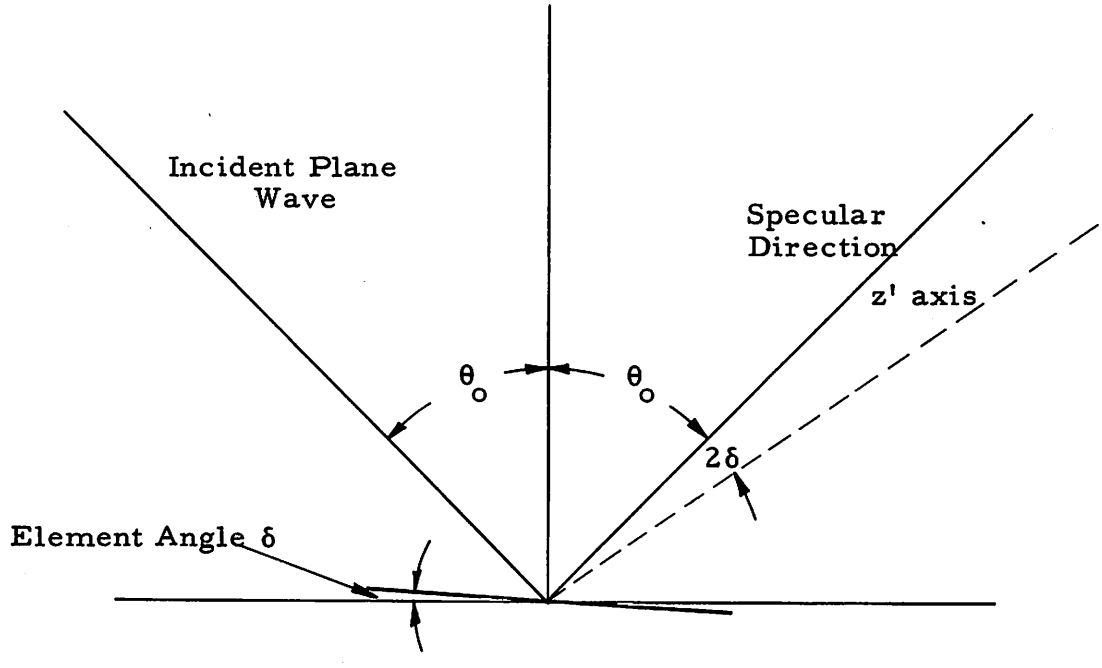

Fig. 12 Relationship between the Plane Wave Source Axis, z', and the Specular Direction

$$dS = ab\, p(\delta)\, d\delta$$

ab represents the portion of x-y plane containing the scatterer, and $p(\delta)$ is the probability density of δ. The probability density of surface slope a has been shown to be[4]

$$p(a) = \frac{1}{\sqrt{2\pi}a_o} \exp\left(-\frac{a^2}{2a_o^2}\right)$$

$$a_o = \sqrt{2}\,\sigma / \xi_{ox}$$

where a_o is the standard deviation of surface slope, σ is the standard deviation of surface height, and ξ_{ox} is the surface correlation distance in the x-direction. For the surfaces under study (Section IV), a_o does not exceed .141, which corresponds to a surface angle δ of about 8^o. Since for δ small, $\delta \approx a$ and $p(\delta) \approx p(a)$, we may write

$$p(\delta) \approx \frac{1}{\sqrt{2\pi}a_o} \exp\left(-\frac{\delta^2}{2a_o^2}\right)$$

Recall that the field pattern of a plane-wave source (Eq. 1) is proportional to $\cos^2(\frac{\theta'}{2})$ and that the angle between $\theta' = 0$, and the specular direction is 2δ. Then the field reduction K_s in the specular direction due to surface slope is given very nearly by

$$K_s = \frac{1}{ab}\int_{-\infty}^{+\infty} ab\, p(\delta) \cos^2(\delta)\, d\delta$$

$$= \frac{1}{\sqrt{2\pi}a_o}\int_{-\infty}^{+\infty} \exp\left(-\frac{\delta^2}{2a_o^2}\right) \cos^2(\delta) d\delta = \frac{1}{2}\left[1 + e^{-2a_o^2}\right]$$

for $a_o = .141$ $K_s = .98$. This corresponds to the roughest surface.

Although the case analyzed above considers the surface rough in only one direction, it should serve to show that the surfaces under study may be considered "gently sloping."

III. 3. The Infinitely-Conducting-Scatterer Approximation

The development of Section II assumed the scatterer to be perfectly-conducting. Water, however, is not a perfect conductor at electromagnetic wave lengths of 8 millimeters. The complex permittivity of 25°C water at 8.6 millimeters is[7]

$$\epsilon' - j\epsilon'' = 21 - j29$$

The reflection coefficient R_H for a horizontally-polarized wave (electric field normal to the plane of incidence), incident at angle θ on a plane boundary between free space and an imperfect dielectric is[8]

$$R_H = \frac{\sin(\pi/2 - \theta) - \sqrt{\epsilon' - j\epsilon'' - \cos^2\left(\frac{\pi/2 - \theta}{2}\right)}}{\sin(\pi/2 - \theta) + \sqrt{\epsilon' - j\epsilon'' - \cos^2\left(\frac{\pi/2 - \theta}{2}\right)}}$$

Figure 13 is a plot of R_H as a function of θ for the values of ϵ' and ϵ'' given above. Reference to this figure indicates that the amplitude and phase of the field scattered by a surface element are functions of the element slope. The maximum standard deviation of slope of the surfaces under study has been shown to be .141, and the fact that the slope distribution is Gaussian means that few elements have slopes that exceed .141. The variation of amplitude and phase of the reflection coefficient as an element takes on slopes of $\pm$ .141 (8°) is also indicated in Fig. 13. Thus the variation of the magnitude of R_H with slope seldom exceeds .05, while the variation of phase with slope seldom exceeds 2°. These figures

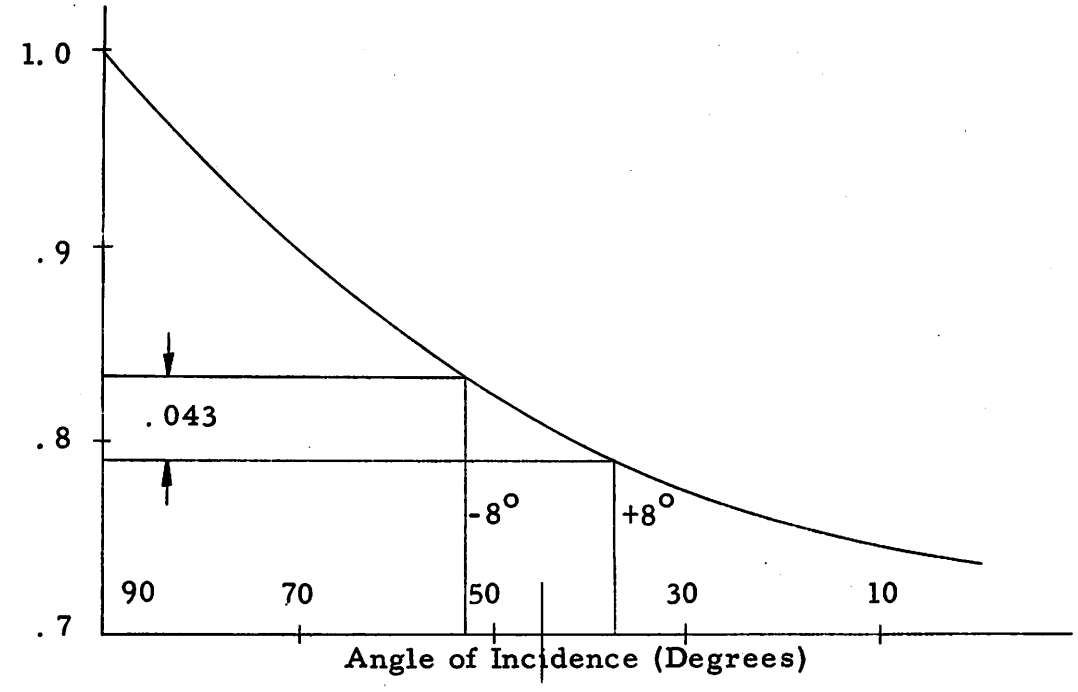

Fig. 13-a Dependence of the Magnitude of the Reflection Coefficient on the Angle of Incidence

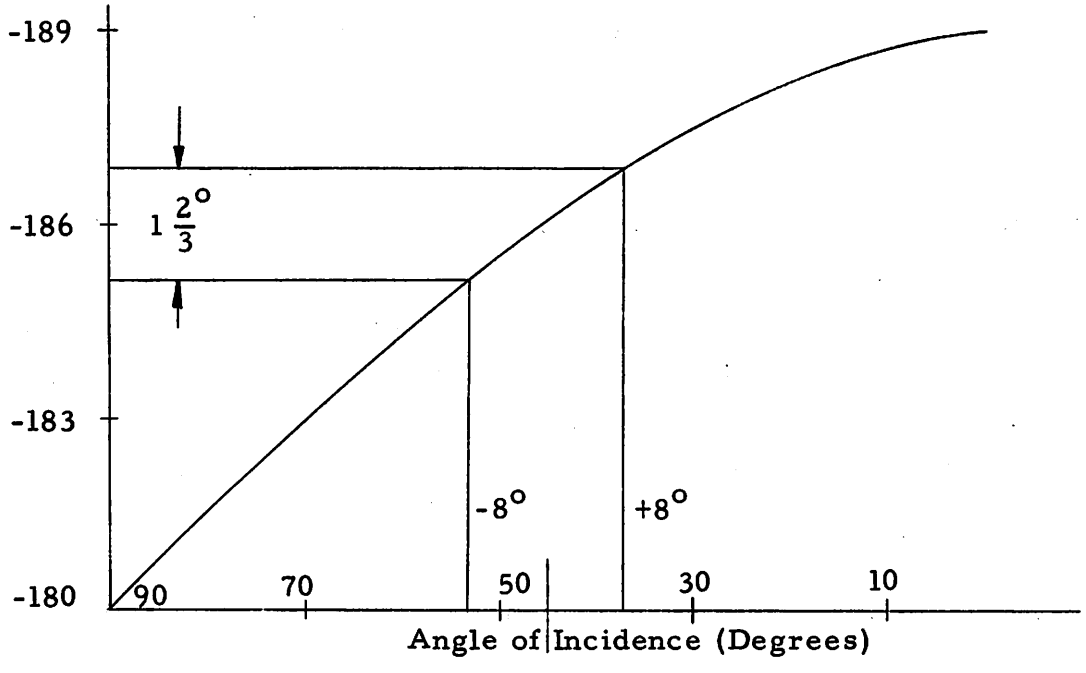

Fig. 13-b Dependence of the Angle of the Reflection Coefficient on the Angle of Incidence

apply to the roughest surface state and are considerably reduced with decreasing surface roughness.

The effect of the variation of the reflection coefficient on the scatter from the surfaces under study is, therefore, small. Thus while the reflection coefficient plays an important role in determining the absolute value of the scattered field, it has only a minor effect on measurements made relative to the smooth-surface-scattered field.

The effect of an imperfectly conducting surface must also be considered in regard to skin depth. If, for example, the incident radiation were to reach the bottom of the ripple tank and be rescattered through the surface, the experimental results would be considerably complicated. The skin depth δ of a material illuminated by a wave of frequency f, and having a permeability μ and a conductivity σ, is

$$\delta = 1/\sqrt{\pi f \mu \sigma}$$

For the surface under study, f = 35 K. M. C. , $\mu = \mu_o = 4\pi \times 10^{-7} \frac{\text{henry}}{\text{meter}}$ $\sigma = \epsilon'' \omega_o = .045 \frac{\text{meter}}{\text{ohm}}$ and $\delta = .37$ mm. Therefore the radiation reaching the bottom of the tank is negligibly small, since the water is 5 cm. deep.

III. 4 Summary of Approximations

In conclusion, it is observed that the only serious limitation of the experimental apparatus is that of the nonuniform illumination of the surface. Because of this limitation it is difficult to use the theory of Section II to predict exactly the absolute value of the variances s_r^2 and s_i^2. The general form of the dependence of these variances on the standard deviation of phase Ψ_o can, however, be checked. The apparatus discussed above is thus a useful approximation to the model analyzed in Section II.

IV. SURFACE MEASUREMENTS

The theory developed in Section II predicts the behavior of specular scatter in terms of $p(z)$, the probability density of surface height, and $\rho(\xi)$, the surface autocorrelation function. The measurement of $p(z)$ and $\rho(\xi)$ is the subject of this section. The results of these measurements are summarized in Table I.

The instantaneous height z of a time-variant rough surface varies in space in a random manner. This variation is described statistically by $p(z)$ and $\rho(\xi)$. These quantities are, in general, a function of position; for the purposes of this discussion, however, the surface will be assumed uniform. That is, $p(z)$ and $\rho(\xi)$ will be assumed independent of position.

To describe completely a time-variant rough surface, the statistical behavior of the time variation must also be considered, This variation is important when it comes to choosing averaging times for time-variant statistical quantities. Suitable averaging times may, however, be estimated by observing the variation in the quantities being averaged. Therefore the statistical behavior of the surface's time variation will not be determined explicitly.

IV.1 The Probability Density of Surface Height

The probability density of surface height, $p(z)$, is given by

$$p(z) = \frac{dP(z)}{dz} \tag{12}$$

where z is the surface height and $P(\epsilon)$ is the probability that the surface height exceeds ϵ. If the surface is uniform and time-variant, $P(\epsilon)$ may be defined as

$$P(\epsilon) = \lim_{T\to\infty} \frac{1}{T} \int_0^T u(t)\, dt \tag{13}$$

where t is time and

$$u(t) = \begin{cases} 0 & z < \epsilon \\ 1 & z > \epsilon \end{cases}$$

$P(\epsilon)$ may also be defined as

$$P(\epsilon) = \lim_{R\to\infty} \frac{1}{R} \int_0^R u(r)\, dr$$

where r is a distance along the surface in any direction and

$$u(r) = \begin{cases} 0 & z < \epsilon \\ 1 & z > \epsilon \end{cases}$$

Once $P(\epsilon)$ is known for all ϵ, $p(z)$ may be determined using Eq. (12). $p(z)$ for a rough-water surface has been measured by Manton,[9] who used photographic techniques to obtain instantaneous surface profiles. The approach here is different. An electronic analog is constructed to perform the operations indicated in Eq. (13). From the plot of $P(z)$ thus obtained, the form of the density function, $p(z)$, and the standard deviation of surface height, σ, are deduced.

The analog used is shown in Fig. 14. This arrangement is seen to consist of a probe which controls an electronic pulsing device whose output is integrated with respect to time. The height of the probe above the mean surface level corresponds to ϵ. When the probe is submerged the grid of the pulsing section tube is at 0 potential. When the probe is out of the water the tube is cut off. The resulting output of the pulsing section is a pulse which corresponds to u(t). That is, when the surface height exceeds ϵ the pulse is on, and when the surface height falls below ϵ the pulse is off. The analog is calibrated by means of S_1 and R_1. S_1 closed corresponds to ϵ equal to $-\infty$, or $P(\epsilon) = 1$. Therefore with S_1 closed, R_1 is adjusted to make the integrator output, V_c, unity. Then with S_1 open, V_c equals $P(\epsilon)$.

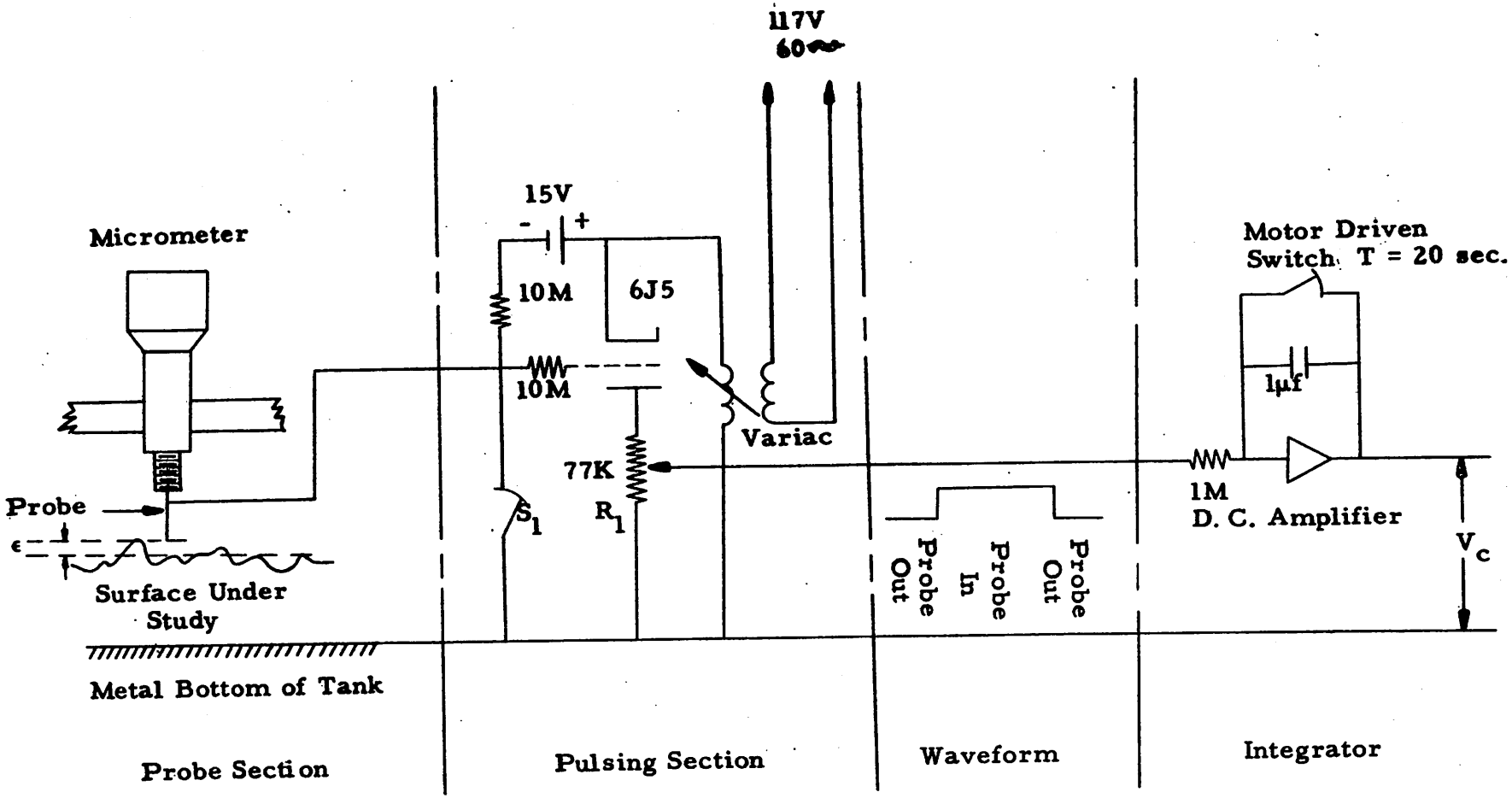

Fig. 14 Schematic of Analog Used to Measure $\rho(\epsilon)$

The surface height seen by the probe is influenced by the meniscus between the probe and the surface. If the probe is set at height ϵ it will make contact with the surface when the surface reaches height ϵ. Due to the meniscus the probe will not break contact until the surface height is $\epsilon - \beta$, where β is the maximum value of the meniscus. The actual surface height sampled, therefore, lies somewhere between ϵ and $\epsilon - \beta$.

Suppose for the sake of argument that the surface made and broke contact with the probe at height $\epsilon - \beta$. The actual surface height sampled would then be $\epsilon - \beta$. If it is assumed that the surface rises in the same manner that it falls, it follows that the "make contact meniscus" and the "break contact meniscus" contribute equally to the reduction in the surface height sampled. Actually, only the "break contact meniscus" exists; therefore the actual height sampled is very nearly $\epsilon - \beta/2$. This relationship is not exact because surface maxima lying in the range ϵ to $\epsilon - \beta/2$ are not sampled. This, however, is a small effect since $\beta/2$ is in practice about .05 millimeters and the standard deviation of surface height of the least rought surface is about .22 millimeters.

In the experimental procedure, β is not determined explicitly; rather, use is made of the fact that

$$P(0) = 1/2$$

where 0 is the co-ordinate of mean surface height as seen by the probe. The probe height is adjusted until V_c is observed to be 1/2 and $P(\epsilon)$ is then measured relative to this height.

Figure 15 shows a typical set of experimental points of $P(\epsilon)$ determined using the methods described above. The solid curve with which these points are compared is a plot of the function

$$P(\epsilon) = \int_{\epsilon}^{+\infty} p(z)\, dz$$

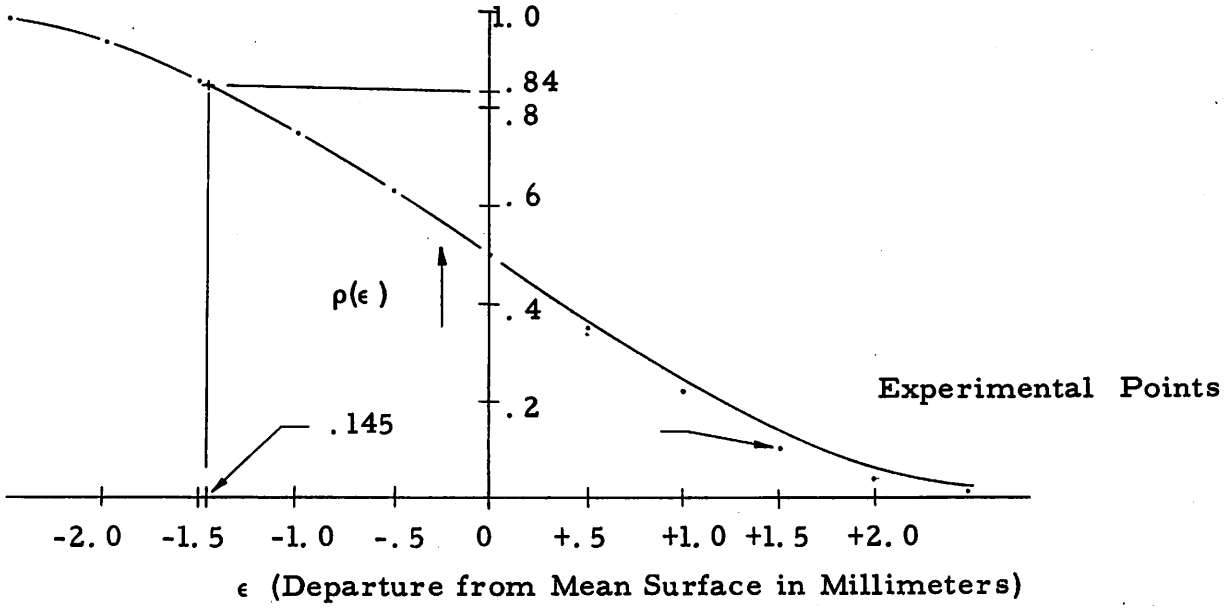

Fig. 15 Comparison Between $\rho(\epsilon)$ Experimental and

$$\rho(\epsilon) = \frac{1}{\sqrt{2\pi}\,1.45} \int_{\epsilon}^{\infty} \exp\left\{\frac{-z^2}{2(1.45)^2}\right\} dz \quad \text{for Roughness V}$$

where

$$p(z) = \frac{1}{\sqrt{2\pi}\,1.45} \exp\left(-\frac{z^2}{2(1.45)^2}\right)$$

is a Gaussian density function having standard deviation 1.45 mm. Close agreement between the experimental points and the curve based on the Gaussian density function indicates that the probability density of surface height of the surface is very nearly Gaussian. The fact that the experimental points fall slightly below the curve for z greater than 0 is due to the fact that surface maxima lying in the range ϵ to $\epsilon - \beta/2$ are not sampled. The effect of not sampling these maxima is to slightly reduce the experimental observations.

The standard deviation of surface height σ can easily be extracted from P(z). Since p(z) is Gaussian and P(0) is 1/2, $P(-\sigma) = .84$ and $P(+\sigma) = .16$. Thus the surface represented

by Fig. 15 has a standard deviation of surface height of 1.45 millimeters. Similar comparisons for the other roughness states studied show that they all had approximately Gaussian distributions of surface height. The results of these comparisons are summarized in Table I at the end of this section. The accuracy with which σ was measured is estimated at $\pm$ .05mm.

IV. 2 The Surface Autocorrelation Function

The autocorrelation function $\rho(\xi)$ is the correlation of surface height between two points separated by a distance ξ. If the surface is time-variant in a uniform manner, $\rho(\xi)$ is given by

$$\rho(\xi) = \lim_{T\to\infty} \frac{\int_0^T z_p(t)\, z_{p+\xi}(t)\, dt}{\int_0^T z_p^2(t)\, dt} \qquad (14)$$

where p is a fixed point on the surface and $p + \xi$ is a second fixed point on the surface separated from p by a distance ξ. $\rho(\xi)$ is also given by

$$\rho(\xi) = \lim_{R\to\infty} \frac{\int_{-R}^{+R} z(r)\, z(r+\xi)\, dr}{\int_{-R}^{+R} z(r)^2\, dr} \qquad (15)$$

where the integral is performed at one instant of time. (i.e., the surface is frozen) Either Eq. (14) or (15) may be used to measure $\rho(\xi)$. Manton,[9] using photographic techniques and hand computation, determined $\rho(\xi)$ through use of Eq. (15). The approach here will be to measure $\rho(\xi)$ using analog techniques to perform the operations of Eq. (14).

A diagram of the analog used is shown in Fig. 16a. This arrangement has two separate channels, 1 and 2, which develop signals proportional to $z_p(t)$ and $z_{p+\xi}(t)$, respectively. These

channels are combined in a function multiplier and the result integrated in a Miller integrator. The probe carriage, Fig. 1>b, provides adjustment of the height ϵ and the probe separation ξ. The probes themselves are excited with alternating current in order to prevent polarization. The impedance between each probe and the bottom of the tank is used as a bridge element. These

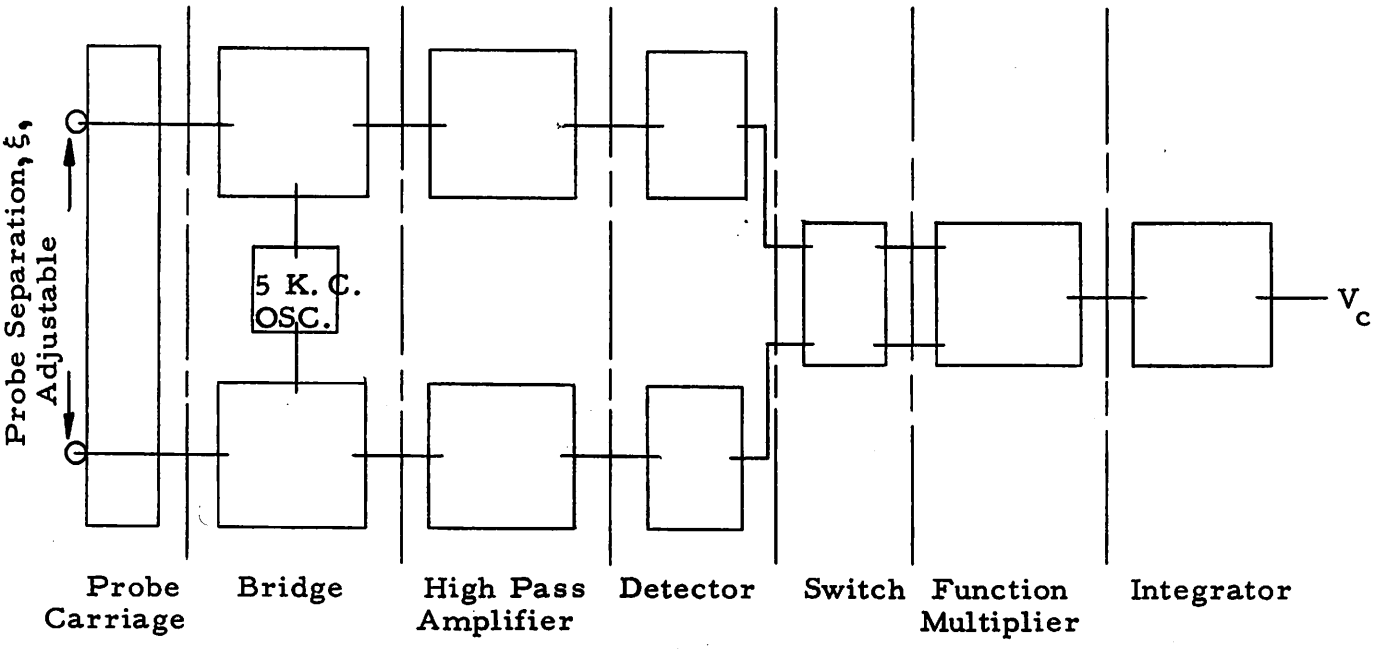

Fig. 16-a Analog for Measuring ρ (ξ)

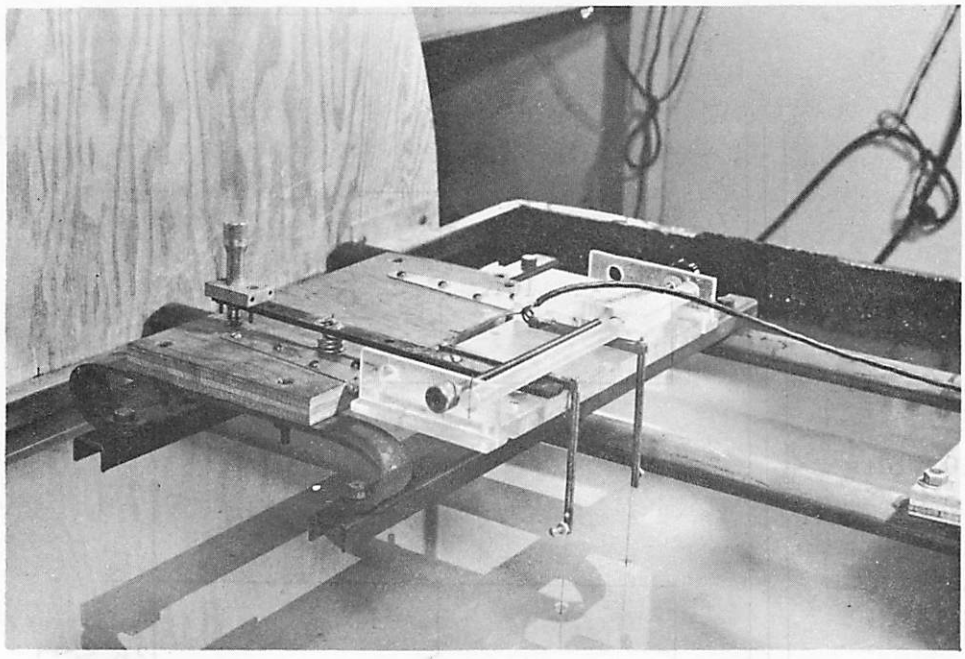

Fig. 16-b. Probe Carriage

impedances can be made a fairly linear function of surface height by proper adjustment of the bridge parameters. * A circuit diagram of the two bridges is shown in Fig. 16c. The output of each bridge is of the form

$$e_B = e_o (1 + kz(t)) \cos (2\pi f t)$$

which is a carrier of frequency f whose amplitude is modulated by the height of the water, z(t), on the probe associated with the bridge in question. The signals thus obtained are amplified in high-pass amplifiers ** which provide the necessary gain but limit excessive

* Actual measurements show the detector output to be linear $\pm$ .1 millimeter over a range of 5 millimeters.

** Narrow-band amplifiers, if available, would have been even better in this application.

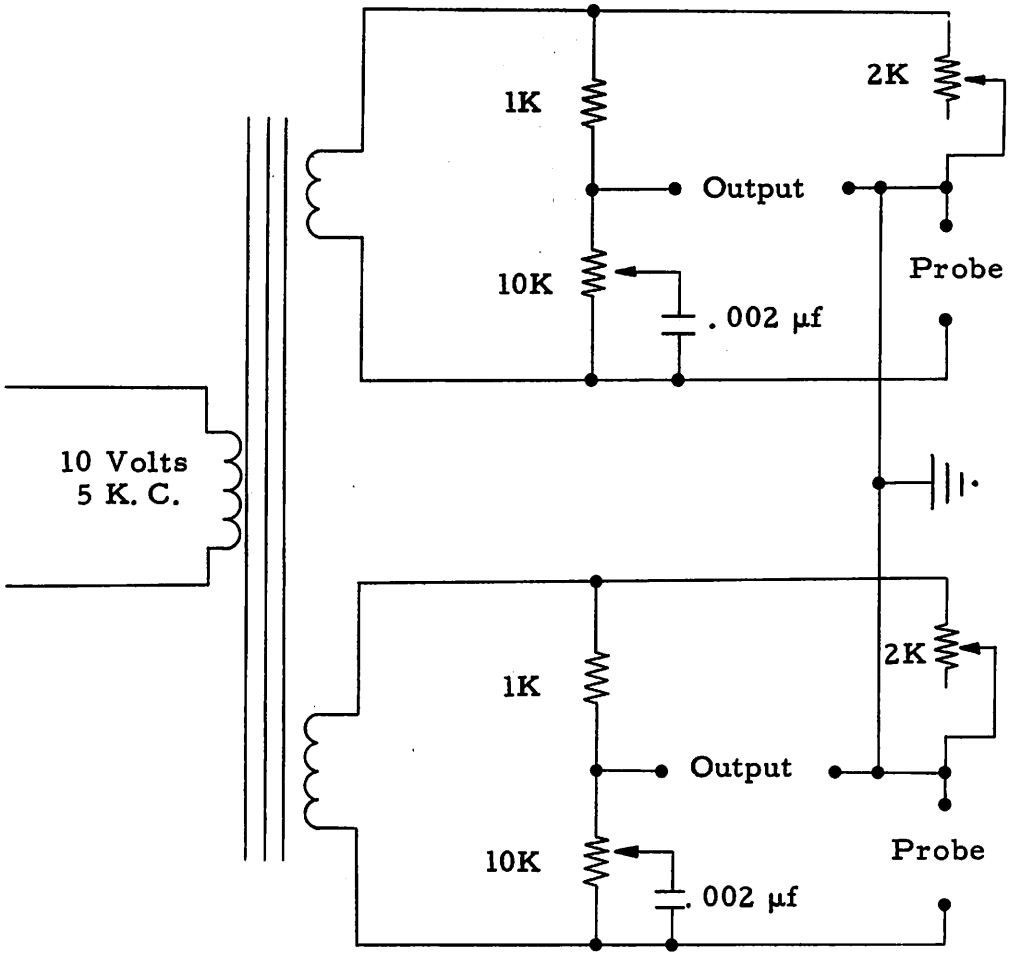

Fig. 16-c Bridge Schematic

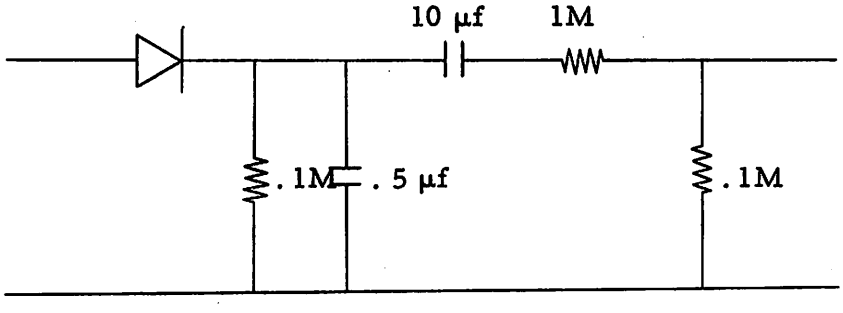

Fig. 16-d Detector Schematic

noise. The amplified signals are then fed to the detectors whose outputs are

$$\left.\begin{aligned} e_1 &= k_1 z_p(t) \\ e_2 &= k_2 z_{p+\xi}(t) \end{aligned}\right\} \qquad (16)$$

The circuit diagram of the detector current used is shown in Fig. 16d. The switching section has three functions. Function 1 produces a signal proportional to e_1^2 at the output of the function multiplier; Function 2 produces a signal proportional to e_2^2 at the output of the function multiplier; and Function 3 produces a signal proportional to $e_1 e_2$ at the output of the function multiplier. The Miller integrator, which is controlled by a motor driven microswitch, provides a 20-second time integral of the output of the function multiplier.

Calibration is necessary only to insure that k_1 and k_2 of Eqs. (16) are equal. This is accomplished by first switching to Function 1, roughening the surface, and measuring the integrator output V_{c1}; then switching to Function 2 and adjusting the gain of channel 2 so that the integrator output V_{c2} associated with Function 2 is equal to V_{c1}.

$\rho(\xi)$ is measured directly by switching to Function 3 and measuring the integrator output V_{c3}. $\rho(\xi)$ is then

$$\rho(\xi) = \frac{V_{c3}}{V_{c1}}$$

V_{c1}, V_{c2}, and V_{c3} used in determining $\rho(\xi)$ are each the result of ten 20-second time integrals and are therefore 200-second averages.

$\rho(\xi)$ has two components $\rho_x(\xi)$ and $\rho_y(\xi)$, where x is the direction along the length of the ripple tank (also the direction of

the exciting air flow) and y is the direction along the width of the tank. By changing the orientation of the probe carriage it was possible to measure both $\rho_x(\xi)$ and $\rho_y(\xi)$. The results of these measurements made at Roughness V are presented in Figs. 17.

The form of the autocorrelation functions is of interest. $\rho_x(\xi)$, the autocorrelation measured in the x-direction, is seen to be very nearly of the form $\exp\left(-\left|\frac{\xi}{\xi_o}\right|\right)$, while $\rho_y(\xi)$, the autocorrelation function in the y-direction, is closer to the form $\exp\left(-\left|\frac{\xi^3}{\xi_o^3}\right|\right)$. $\rho_x(\xi)$ and $\rho_y(\xi)$ were found to maintain these forms over the whole range of surface variations measured. The difference in these forms is probably due to the method by which the surface was excited, the method of excitation being air-blown over the surface in the x-direction. The form of autocorrelation functions in general is discussed by Chernov,[10] who shows that a bounded function may not have an autocorrelation function of the form $\exp\left(-\left|\frac{\xi}{\xi_o}\right|\right)$. Chernov points out, however, that autocorrelation functions of this form are commonly measured. A summary of the autocorrelation functions measured for the experimental surfaces in question is presented in Table I. The accuracy of these measurements is estimated at $\pm$ .25 cm.

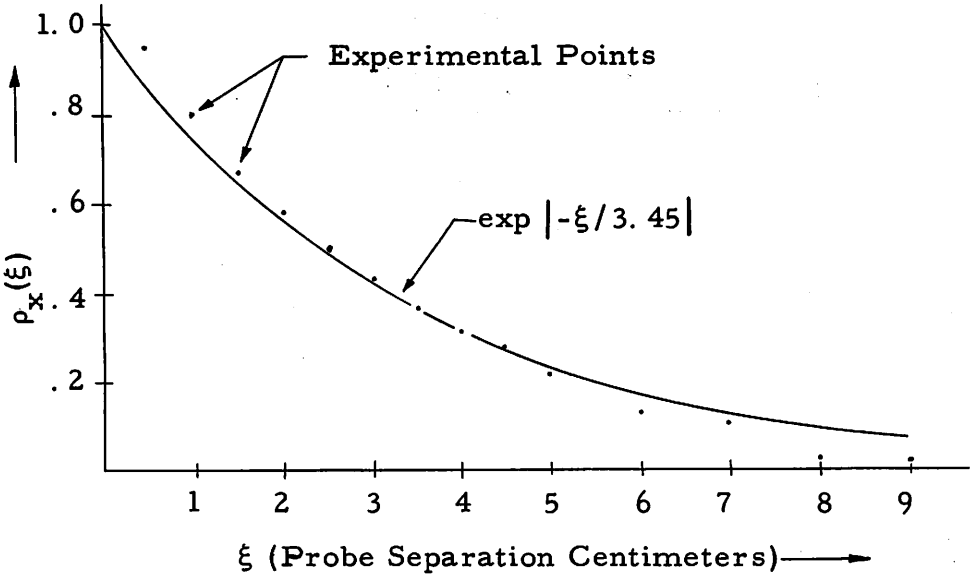

Fig. 17-a Autocorrelation Function $\rho_x(\xi)$ for Roughness V

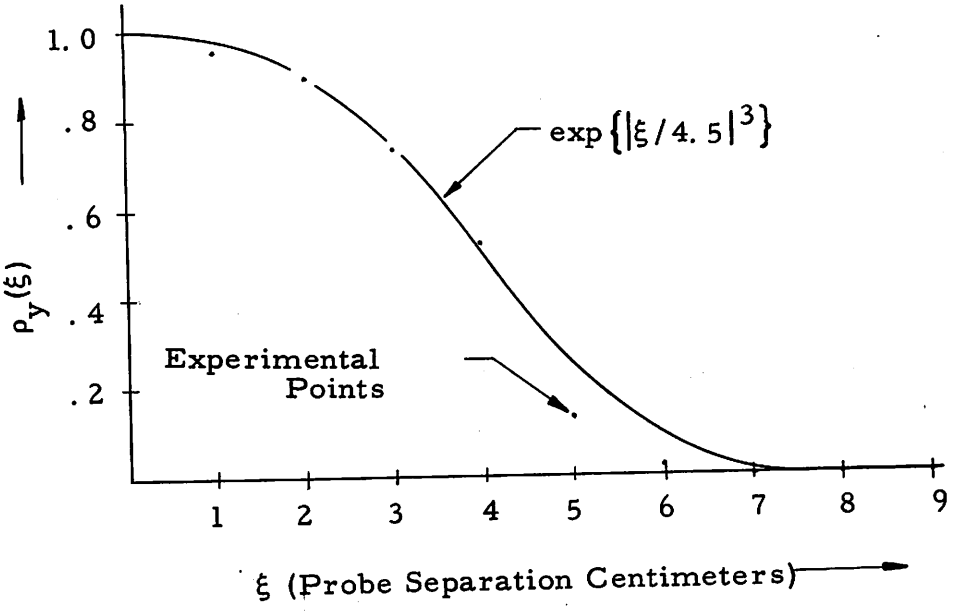

Fig. 17-b Autocorrelation Function $\rho_y(\xi)$ for Roughness V

TABLE I

SUMMARY OF SURFACE MEASUREMENTS

Roughness	σ mm[++]	ρ_x cm[+++]	ρ_y cm[+++]
I	.22	6.5 cm	3.0 cm
II	.30	5.6 cm	+
III	.56	5.1 cm	+
III 1/2	.72	+	+
IV	.96	3.8	+
IV 1/2	1.14	+	+
V	1.45	3.4 cm	3.6 cm
V 1/2	1.66	+	+
VI	2.00	3.0	+
VI 1/2	2.35	+	+
VII	2.70	+	+
VIII	3.00	2.9 cm	4.5 cm

\+ not measured

++ all measurements of $\sigma \pm .05$ mm

+++ all measurements of $\rho \pm .25$ cm

V. MEASUREMENT OF SPECULAR SCATTER

The theory developed in Section II predicts the behavior of specular scatter from a rough surface. The purpose of this section is to compare actual scattering measurements with this theory. The scattering measurements are made on the rough-water surface described in Section IV; the experimental apparatus was discussed in Section III.

The scattered field predicted in Section II depends on the surface roughness and on the number of surface variations illuminated. The surface roughness is controlled and measured as described in Section IV. The number of surface variations illuminated is varied by using two parabolic reflectors, one 30 inches in diameter, the other 10 inches in diameter. Since the surface is close to the parabolic reflectors, the 30-inch parabola was found to illuminate more surface area than the 10-inch parabola. It is thus possible to vary the number of surface variations illuminated.

The measurements themselves are presented in two sections. The first section presents measurements of time-average power made with both the 10-inch and the 30-inch reflectors. These are then compared with Eq. (11) which is the theoretical expression for time-average power. The second section presents measurements of the time-average power associated with the phase quadrature random field components E_r' and E_i. These measurements are compared with the theoretical predictions of Figs 8. This second set of measurements is made only with the 10-inch reflector. The electric field is horizontally polarized (parallel to the surface) in all of the above measurements.

V.1 Measurement of Time-Average Power

The measurement of time-average power was made with the apparatus discussed in Section III and with the circuit shown in Fig. 18. The microwave energy which illuminates the surface is

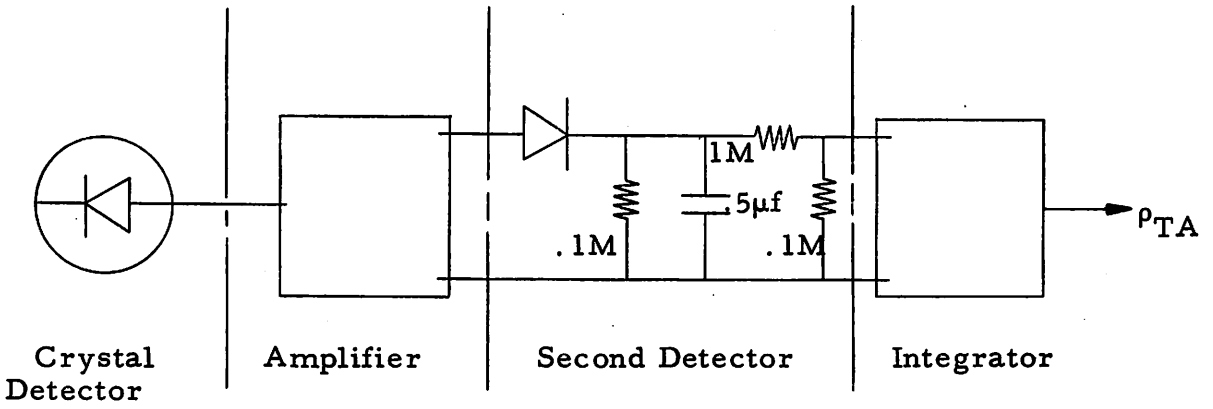

Fig. 18 Circuit Used for Measuring Time Average Power

100 % modulated by a 1-kilocycle-square wave. The portion of this energy which is scattered to the receiving point is received by an open end of waveguide. This waveguide is connected to a precision attenuator which adjusts the received signal level to be within the square law range of the crystal. (This range was about 25 decibels for the crystal used.) The output of the crystal is a 1-kilocycle carrier whose amplitude is proportional to the instantaneous power received from the surface. This signal is amplified and the 1-kilocycle carrier removed by the detector. The detector output, which is directly proportional to the instantaneous power, is then integrated with respect to time in order to obtain an output proportional to the time-average power. The integrator is controlled by a motor-driven microswitch which provides twenty-second integration times.

The system linearity was checked by adding known amounts of attenuation by means of the precision attenuator which preceeds

the crystal detector. The system was found to be linear to within + 0% to -2% for integrator outputs of 100 volts to 1 volt. The system gain was then adjusted so that the integrator output corresponding to a smooth surface was 100 volts and the normalized time-average power was measured by roughening the surface and noting the reduction in the integrator output. The actual power reduction was determined by averaging the results of 10 twenty-second integrations; therefore the experimental points represent 200-second averages.

The normalized time-average power associated with each of the roughness states summarized in Table I was measured for both the 30-inch reflector and the 10-inch reflector. The results of these measurements plotted as functions of the standard deviation of phase Ψ_o are presented in Figs 19 and 20. Figure 21a is a plot of the difference between the experimental points obtained using the 10-inch reflector and the curve $\exp\left(-\Psi_o^2\right)$. According to Eq. (11) this is just the normalized incoherent power $s_r^2 + s_i^2$.

The theoretical normalized time-average power, P_{ta}, given by Eq. (11), is

$$P_{ta} = \exp\left(-\Psi_o^2\right) + s_r^2 + s_i^2 \qquad (11)$$

This expression shows that the time-average power is composed of a "coherent" term $\exp\left(-\Psi_o^2\right)$ and a "noise term" $s_r^2 + s_i^2$. The standard deviation of phase Ψ_o can be computed immediately from Eq. (3-b).

$$\Psi_o = 2\,k\,C_o\,\sigma \qquad (3\text{-}b)$$

where k is the free space propagation constant $\frac{2\pi}{\lambda}$; C_o is the cosine of the angle of incidence; and σ is the standard deviation of surface height. The average angle of incidence is 45^o and the electromagnetic wavelength is 8.40 millimeters. Ψ_o is therefore

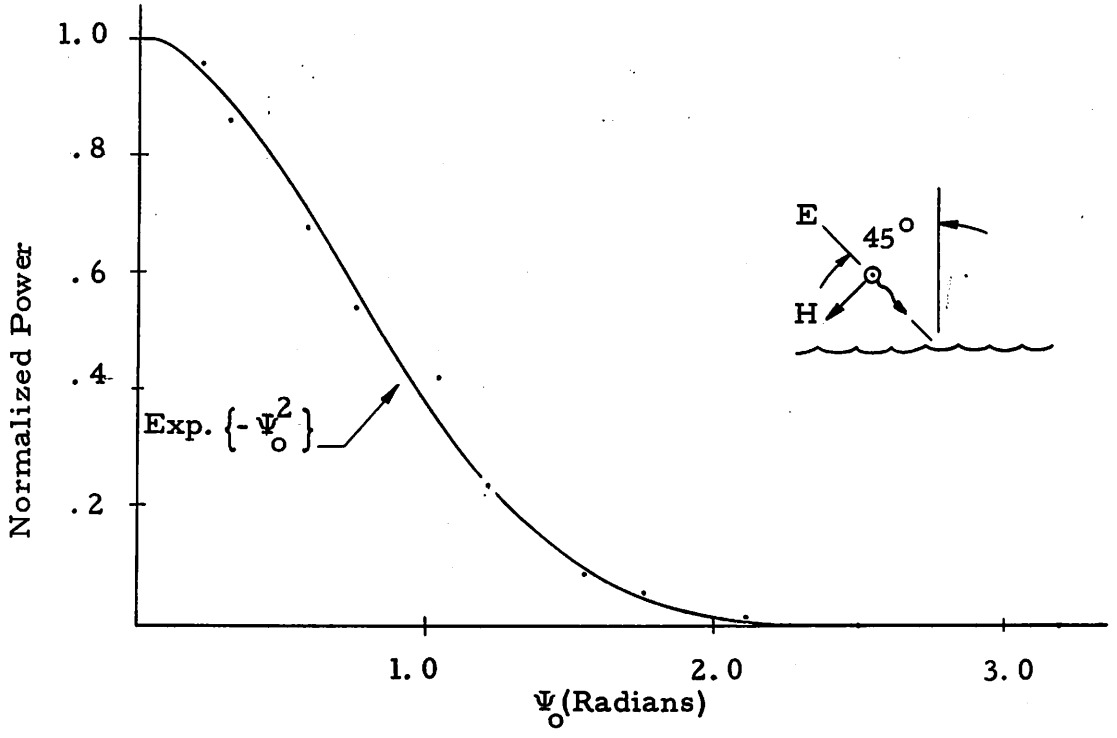

Fig. 19 Normalized Power vs. Standard Deviation of Phase for the 30 Inch Parabola

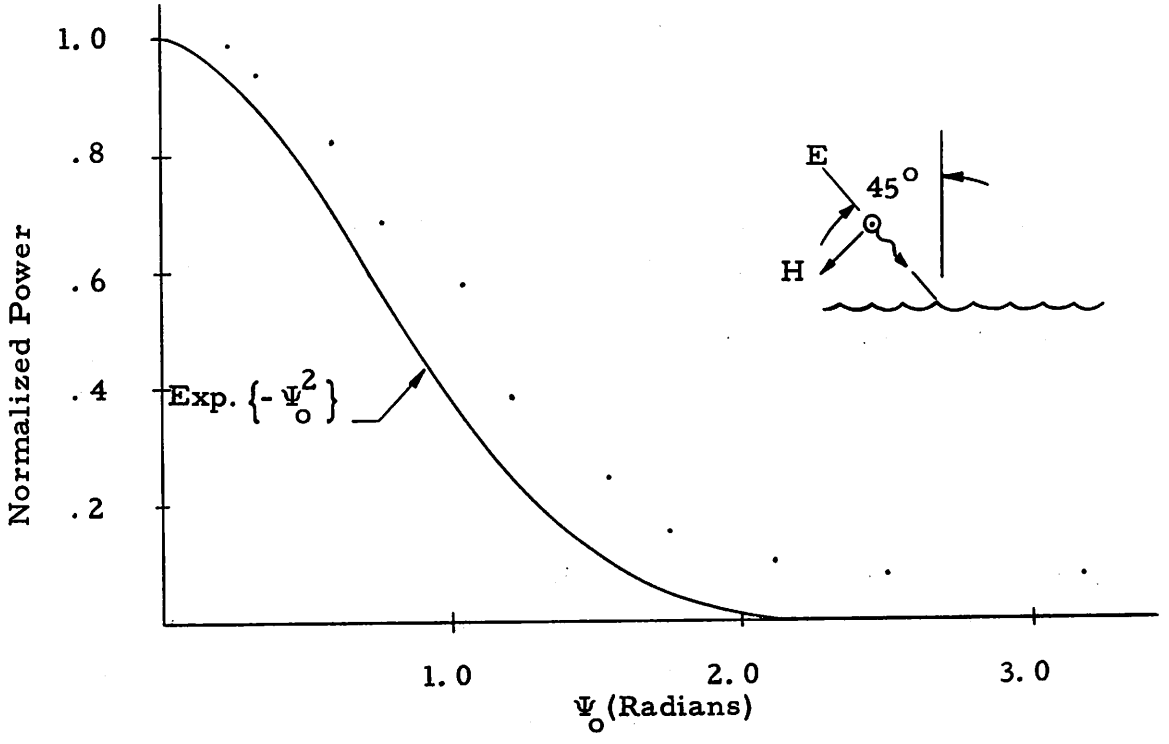

Fig. 20 Normalized Power vs. Standard Deviation of Phase for the 10 Inch Parabola

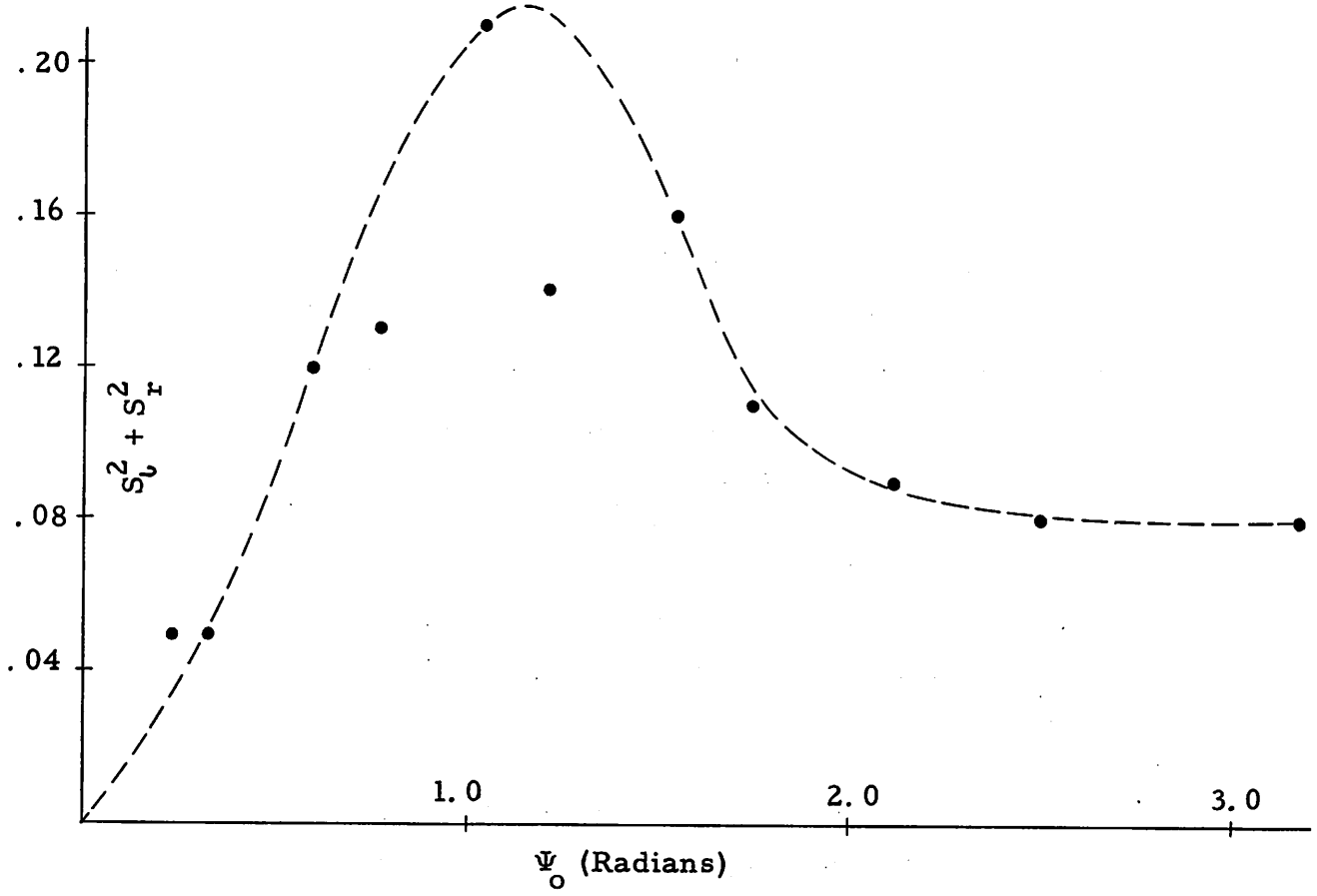

Fig. 21-a $S_v^2 + S_r^2$ Experimental (10 Inch Parabola)

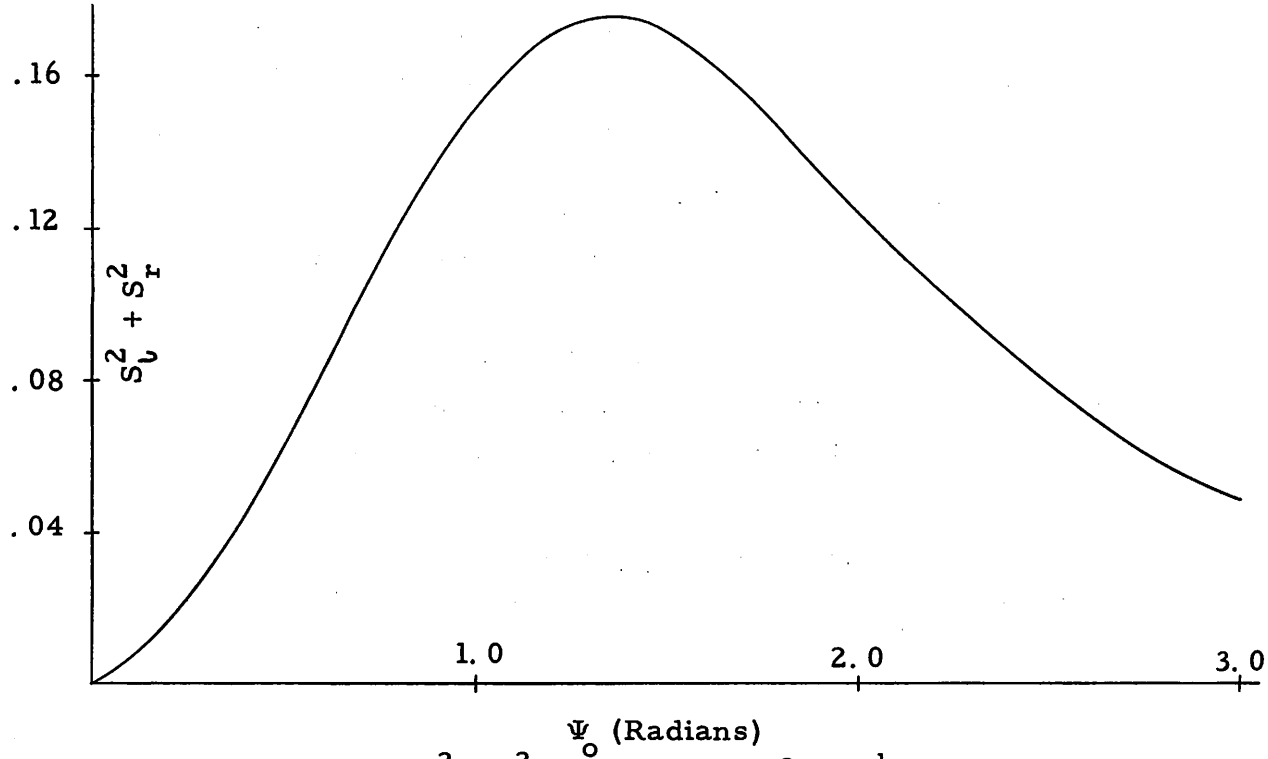

Fig. 21-b $S_v^2 + S_r^2$ Theoretical ($\frac{a}{\xi_{ox}} = \frac{b}{\xi_{oy}} = 2$)

given by

$$\Psi_o = 1.06\,\sigma$$

where σ is the standard deviation of surface height in millimeters. Ψ_o may now be determined for any roughness state by reference to Table I, which lists σ for the different roughness states studied.

As pointed out in Section III, it is not feasible to determine s_r^2 and s_i^2 exactly; the following order of magnitude argument must therefore suffice to gain an idea of the size of these quantities. The first nulls of the surface illumination from the 30-inch reflector were measured and found to be separated by 15 centimeters in both the x- and y-directions. (As before, the x-direction is taken along the tank and the y-direction is taken across the tank.) Since from Table I ξ_{ox} and ξ_{oy} are seen to average about 3 centimeters, the illuminated surface is roughly equivalent to a uniformly illuminated rectangular rough scatterer having dimensions a by b with $a/\xi_{ox} = b/\xi_{oy} = 5$. Reference to Fig. 8c indicates the dependence on Ψ_o of s_i^2 and s_r^2 for such a scatterer. A similar order of magnitude argument shows that the surface illuminated by the 10-inch reflector is roughly equivalent to a uniformly illuminated rectangular scatterer having dimensions a by b with $a/\xi_{ox} = b/\xi_{oy} = 2$. Reference to Fig. 8b indicates the dependence on Ψ_o of $s_i^2 + s_r^2$ for such a scatterer.

The coherent term of Eq. (11), $\exp\left(-\Psi_o^2\right)$, is now known.* The noise term of Eq. (11), $s_i^2 + s_r^2$, is known approximately and depends on the reflector used. It is thus possible to make a prediction of the time-average power scattered by both the 30-inch reflector and the 10-inch reflector. Let us now compare the measured

*The accuracy with which this term is known depends upon the accuracy with which σ can be measured. This accuracy is about $\pm$ .05 millimeters.

values of time-average power with these predictions.

In Fig. 19 the experimental points of time-average power measured using the 30-inch reflector are presented. Also plotted in Fig. 19 is the coherent term of Eq. (11), $\exp\left(-\Psi_o^2\right)$. Close agreement between the experimental points and this curve is evident. The fact that the experimental points are given very nearly by the coherent term of Eq. (11) indicates that the noise term $s_r^2 + s_i^2$ must be small. The approximate dependence of $s_i^2 + s_r^2$ on Ψ_o for the 30-inch reflector is given in Fig. 8c. Reference to this figure shows that the maximum theoretical value of $s_r^2 + s_i^2$ is .053. This is in good agreement with the conclusion reached above, namely, that $s_i^2 + s_r^2$ is "small." According to Eq. (11) the time-average power always exceeds $\exp\left(-\Psi_o^2\right)$. The fact that some experimental points fall slightly below this value is attributed to experimental error. The significance of the above measurement is that it shows that the time-average power is given very nearly by $\exp\left(-\Psi_o^2\right)$ if the scatterer is composed of "many" surface variations. It is also significant that the theory of Section II is able to give a quantitative meaning to "many" surface variations.

In Fig. 20 the experimental points of time-average power measured using the 10-inch reflector are presented. Also plotted in Fig. 20 is the coherent term of Eq. (11), $\exp\left(-\Psi_o^2\right)$. All of the experimental points exceed this curve; some exceed it by a considerable amount. According to theory (see Eq. 11), the amount by which the experimental points exceed $\exp\left(-\Psi_o^2\right)$ is $s_r^2 + s_i^2$. Thus $s_r^2 + s_i^2$ may be determined by taking the difference between the experimental points and the curve $\exp\left(-\Psi_o^2\right)$. $s_r^2 + s_i^2$ measured in this way is presented in Fig. 21a. The approximate theoretical behavior of $s_r^2 + s_i^2$ for the 10-inch reflector is plotted in Fig 21b, which is taken directly from Fig. 8b. It will be recalled that the predicted theoretical behavior of $s_r^2 + s_i^2$ was based on the assumption that the surface illuminated by the 10-inch

reflector could be approximated by a uniformly illuminated rectangular rough scatterer having dimensions a by b with $a/\xi_{ox} = b/\xi_{oy} = 2$, where a and b were taken as the distances between the first nulls of the surface illumination in the x- and y-directions respectively. This assumption is somewhat arbitrary and therefore while the apparent agreement in magnitude between the experimental and theoretical curves of Fig. 21 is encouraging, it must be taken for what it is--a rough approximation. The agreement in Figs. 21 that is more significant is that of the form of $s_r^2 + s_i^2$. Both the theoretical and the experimental curves are seen to rise from 0 and reach a maximum in the neighborhood of $\Psi_o = 1$ radian. For greater values of Ψ_o, both curves are seen to decrease. Examination of Figs. 8a-b-c indicates that $s_r^2 + s_i^2$ has this same general dependence of Ψ_o, regardless of the number of surface variations composing the scatterer. Thus the above rough approximation as to the size of the scatterer should not affect the form of these curves. The fact that the form of the curves of Fig. 21 do not agree exactly is attributed to experimental error. In particular, it appears that the experimental curve flattens out for Ψ_o above 2.5, while the theoretical curve continues to decrease. The explanation of this effect is probably due to the fact that the 10" parabola was not constructed with the necessary accuracy to obtain a good focus at 8-millimeter wavelengths. Purposely defocusing the 30" parabola produced a similar effect.

The above measurement is significant. In the first place, it shows that the effect of reducing the number of surface variations illuminated is to make the normalized time-average power exceed $\exp - \Psi_o^2$. Secondly, it shows that this increase may be interpreted as $s_i^2 + s_r^2$, whose form may be predicted by the theory of Section II. It also tends to indicate that the magnitude of $s_r^2 + s_i^2$ may be approximated by considering the scattering surface to be a uniformly-illuminated rough scatterer of dimensions a by b, where a and b are the distances between the first nulls of the surface illumination in the x- and y-directions, respectively. This last point could be of considerable practical interest and therefore might be worthy of further investigation.

The above-described measurements argue strongly for the validity of Eq. (11) and the theory on which it is based. The remaining theoretical point which must be checked is the magnitude of s_r^2 relative to s_i^2. This is the subject of the next section.

V.2 Measurement of s_r^2 Relative to s_i^2

In Section II it was seen that the instantaneous normalized field was made up of a coherent component $\exp\left(-\frac{\Psi_o^2}{2}\right)$ and the two random-phase-quadrature components E_r' and E_i. E_r' was in phase with the coherent component and its variance was s_r^2. E_i was in phase quadrature with the coherent component and its variance was s_i^2. Reference to Figs. 8 indicates that s_i^2 and s_r^2 are not equal. This section describes a measurement of s_r^2 relative to s_i^2.

A microwave bridge was constructed as illustrated in Fig. 22. The power in the reference arm of this bridge was adjusted to be about 100 times the power scattered from the surface when the surface is smooth. The ratio of the reference arm field to the smooth surface, scattered field is thus 10 to 1. By adjusting the field in the reference arm, E_1, to be in phase with the coherent component from the surface, the variation in the magnitude of the resultant field could be made approximately equal to E_r'. This is illustrated in Fig. 23a. E_i is, of course, still present but since it is in phase quadrature with the large added field component, the variation in the magnitude of the total field due to E_i is small. Alternately, the phase of the reference field E_1 can be adjusted to produce the relationship illustrated in Fig. 23b. In this case the constant part of the resultant field is in phase with the random component E_i. Thus the variation in the magnitude of the resultant field is very nearly the variation of E_i. The variation in the magnitude of the resultant field produced by E_r' is small compared to the variation produced by E_i, because

field variations in phase quadrature with the large constant field have negligible effect on the magnitude of the resultant field.

The magnitude of the total field at the crystal is in general the sum of a constant component E_k and a random time-varying component E_v. Since the crystal detector is operated in its square-law range, its output V_x is

$$V_x = (E_k + E_v)^2 = E_k^2 + 2E_kE_v + E_v^2$$

E_k is merely the magnitude of the vector sum of the coherent scattered field $\exp\left(-\frac{\Psi_o^2}{2}\right)$, and E_1 the field in the reference arm of the bridge. If E_1, which is measured relative to the smooth-surface-scattered field, is very much greater than 1, E_k is practically independent of the coherent scattered term, $\exp\left(-\frac{\Psi_o^2}{2}\right)$. As discussed above, E_v can be made approximately equal to either E_r or E_i by adjusting the phase of E_1. The results of the last section indicate that $s_i^2 + s_r^2$ was much less than 1 even for the 10-inch reflector. Thus E_r^2 and E_i^2 must also be much less than 1, and very much less than E_k, which is approximately 10. Therefore it is possible to approximate the above expression for V_x by

$$V_x \approx E_k^2 + 2E_kE_v$$

The fact that E_k is practically independent of $\exp\left(-\frac{\Psi_o^2}{2}\right)$ means that the second term of this expression is proportional only to E_v.

The time average of E_v^2 is measured with the circuit illustrated in Fig. 24. After amplification V_x is detected and the constant (time-average) component E_k^2 removed by a blocking condenser. The output of the blocking condenser which is proportional to E_v is squared by the function multiplier and integrated with respect to time. The integrator output is therefore proportional to the time average of E_v^2. Thus in the case where

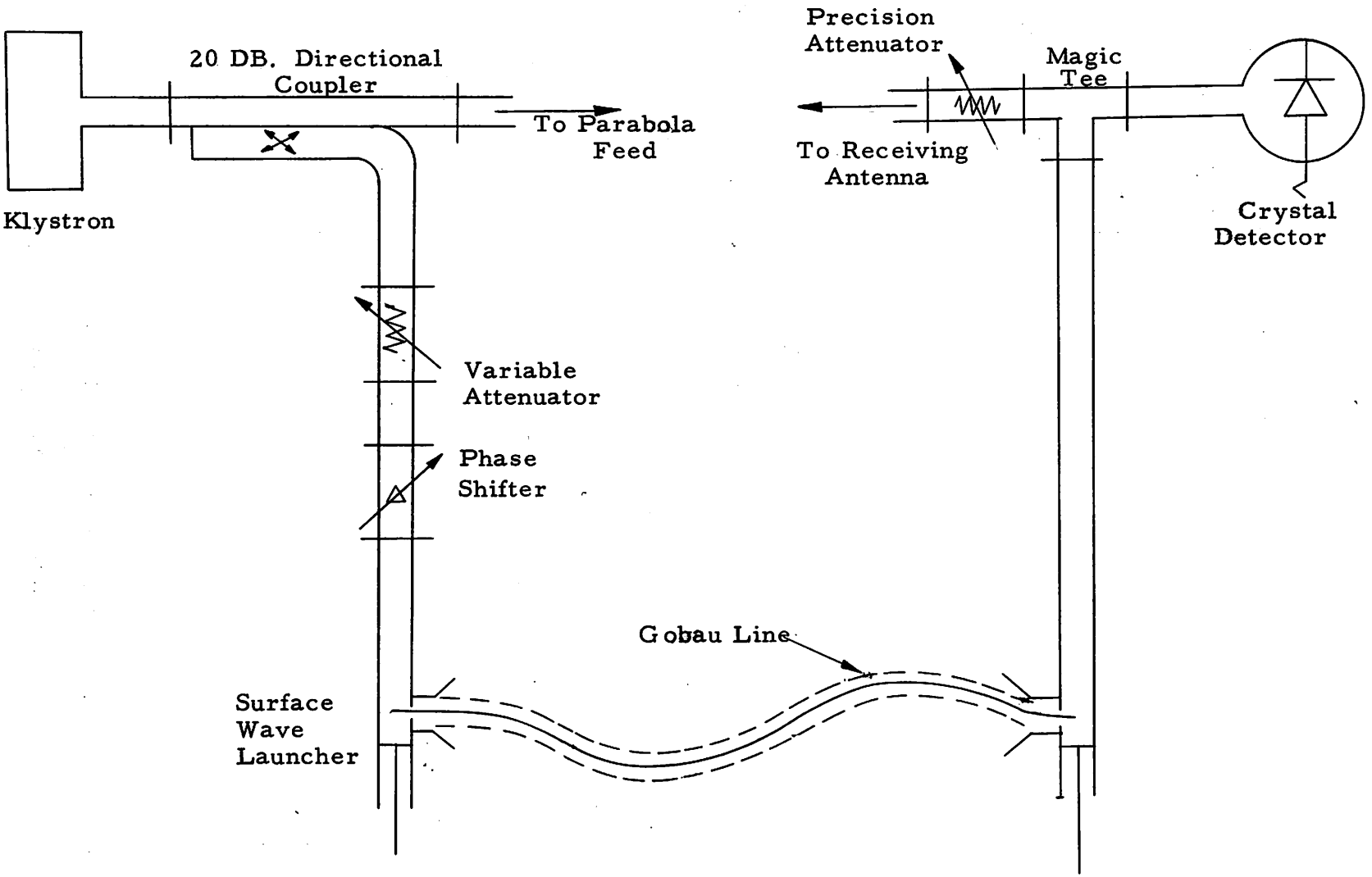

Fig. 22 Microwave Bridge Used to Measure E'_r and E_i

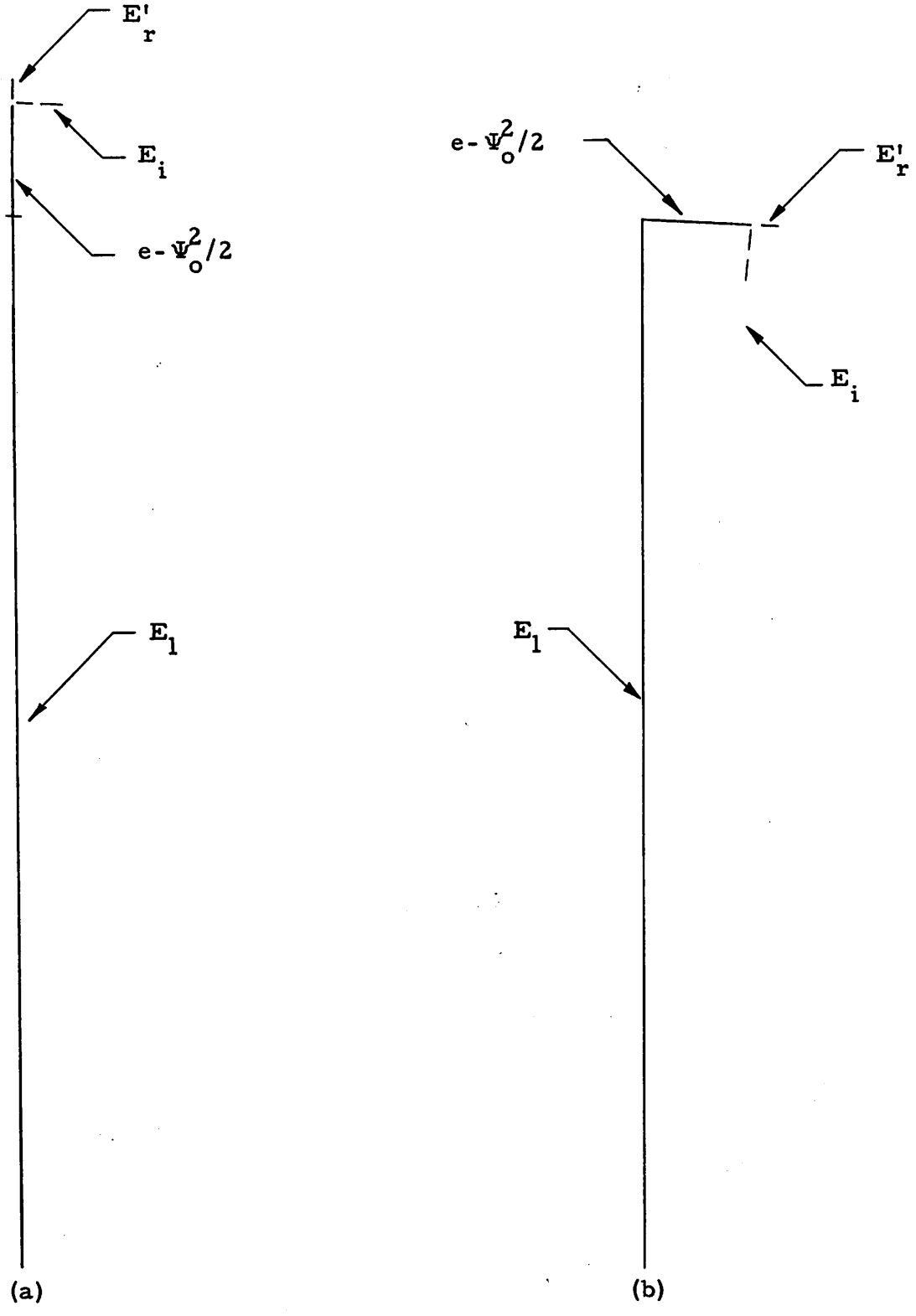

Fig 23 Phasor Diagram Illustrating the Relationship between the Field Components at the Crystal

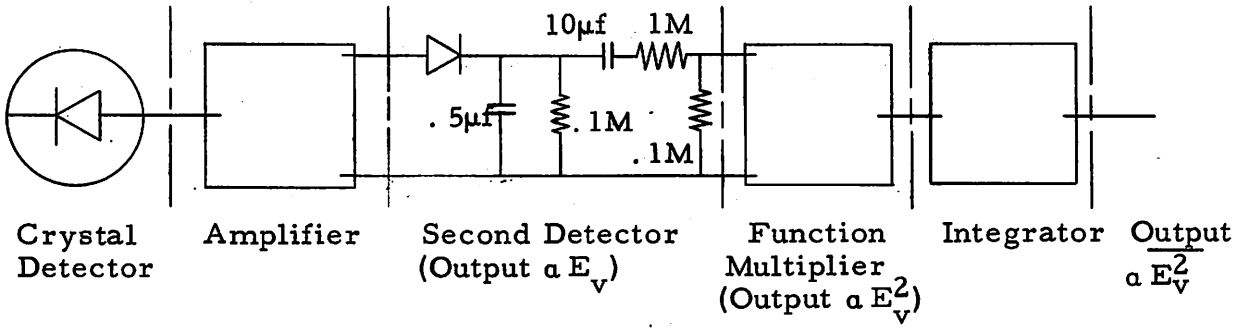

Fig. 24 Circuit Used to Measure $\overline{E'^2_r}$ and $\overline{E^2_v}$

$E_v = E_i$;the integrator output is proportional to s_i^2; when $E_v = E_r$ the integrator output is proportional to s_r^2.

s_r^2 and s_i^2 were measured as described above and the results presented in Fig. 25a. Figure 25b, which is a reproduction of Fig. 8b, gives the theoretically predicted behavior of s_r^2 and s_i^2. General agreement between the theory and the measurements is observed. Agreement is also noted with the measurements of $s_r^2 + s_i^2$ made in the last section. Despite the general agreement, s_r^2 is seen to increase more rapidly than would be expected in the neighborhood of $\Psi_o = 0$. It is also noted that s_r^2 and s_i^2 do not have exactly the same values at 3 radians as predicted by the theory. These discrepancies are attributed to experimental error.

The above measurement is significant because it shows that the noise component of the scattered signal is non-Rayleigh; that is, $s_r^2 \neq s_i^2$.

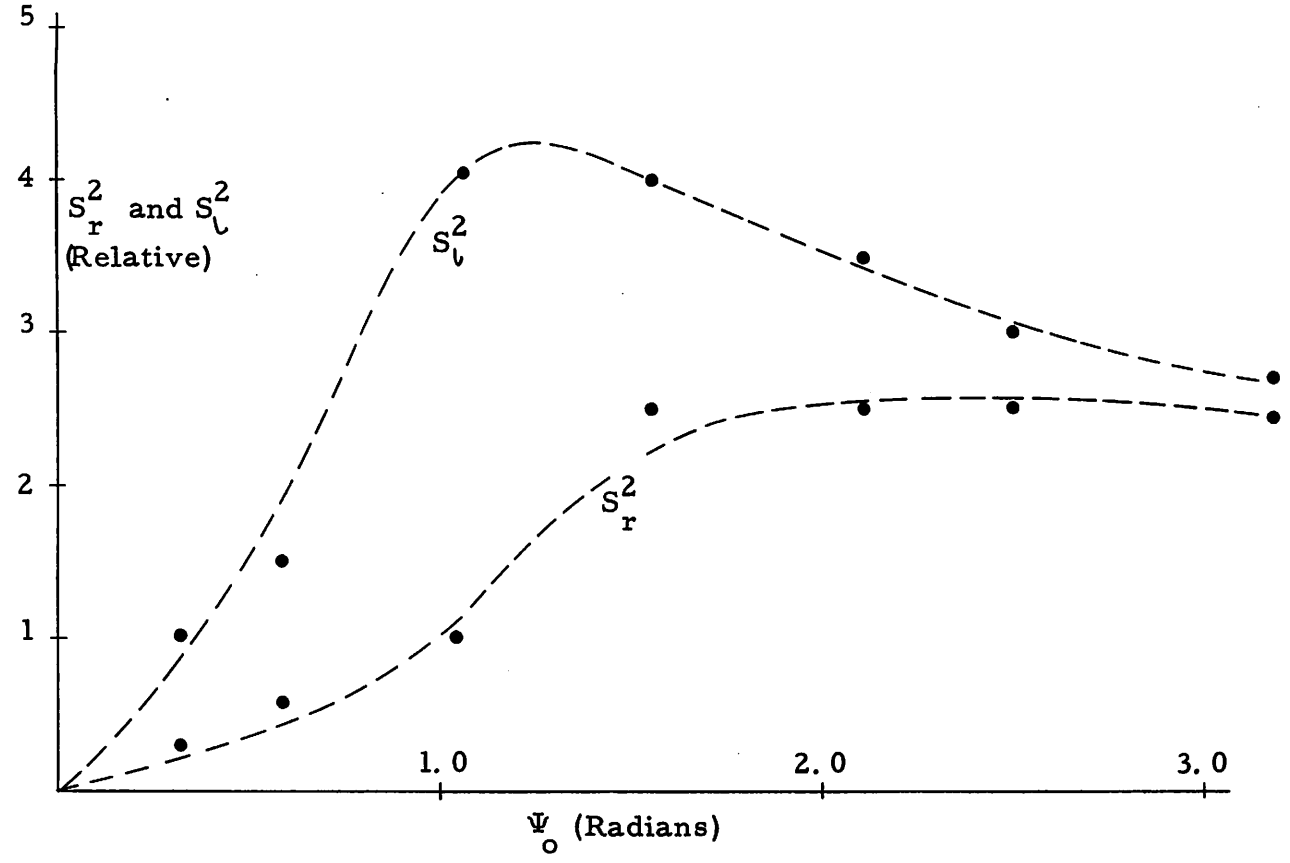

Fig. 25-a S_ι^2 and S_r^2 Experimental (10 Inch Parabola)

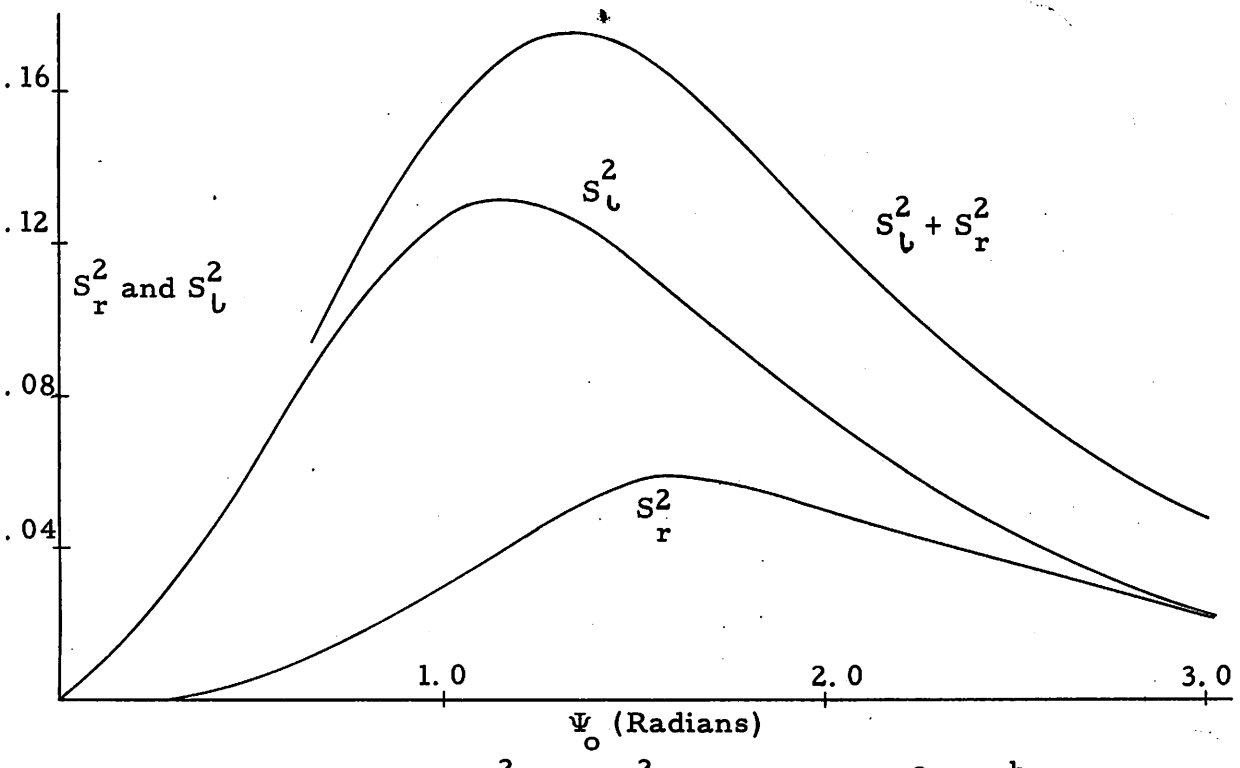

Fig. 25-b S_ι^2 and S_r^2 Theoretical ($\frac{a}{\xi_{ox}} = \frac{b}{\xi_{oy}} = 2$)

V. 3 Summary of Electromagnetic Measurements

The foregoing measurements confirm the theory of Section II. Theory predicts that if the scatterer is composed of many surface variations the normalized time-average power scattered by it is very nearly $\exp(-\Psi_o^2)$. This was measured and found to be the case. Theory further predicts that if the scattering surface is composed of only a few surface variations the normalized time-average power will substantially exceed $\exp(-\Psi_o^2)$. This was also found to be the case. The increase over $\exp(-\Psi_o^2)$ of the normalized time-average power was measured and found to have the same Ψ_o dependence as $s_r^2 + s_i^2$ predicted by theory. It was therefore concluded that this increase could be interpreted as the "noise power term" $s_r^2 + s_i^2$ of Eq. (11). The magnitude of the noise power term could not be predicted exactly because of the nonuniform surface illumination. An order of magnitude approximation, however, was found to predict the noise power surprisingly closely. The magnitude of s_r^2 relative to s_i^2 was measured and found to agree closely with the theory of Section II.

Where exact correspondence with theory was not observed, the differences are within experimental error. The above measurements thus strongly substantiate the theory of Section II.

VI. CONCLUSION

The foregoing theoretical development and measurements indicate that the specular scatter from a time-variant rough surface is dependent both on the surface roughness (standard deviation of surface height) and on the number of surface variations illuminated. If many surface variations are illuminated the scattered field is very nearly constant. This constant is the smooth-surface-scattered field reduced by $\exp\left(-\frac{\Psi_o^2}{2}\right)$. If only a few surface variations are illuminated the scattered field becomes time-variant and may be considered to be composed of a "coherent" (time-average) component and two-phase-quadrature "noise" (random-time-variant) components. The coherent component is the smooth-surface-scattered field reduced by $\exp\left(-\frac{\Psi_o^2}{2}\right)$. The noise components depend on both the surface roughness and the number of surface variations illuminated.

The dependence of the noise components on the size of the illuminated surface, the standard deviation of surface height σ, and on the surface autocorrelation function $\rho(\xi)$ has been theoretically predicted and the validity of these predictions has been experimentally verified. The magnitude of the noise components depends on the number of surface variations illuminated. If many surface variations are illuminated the noise components are small. As the number of surface variations illuminated is decreased the noise components increase. The dependence of the noise components on the surface roughness is of particular interest. As the surface roughness is increased from zero the noise components also increase from zero. When the standard deviation of phase produced by the rough surface is about one radian, the noise components reach their maximum values. Beyond this point the noise components decrease with increasing surface roughness.

The two-phase-quadrature noise components contain equal power only when the standard deviation of phase exceeds three

radians. For smaller standard deviations of phase the noise component in phase with the coherent component contains less power than the noise component in phase quadrature with the coherent component. The scatter from a time-variant rough surface may therefore by thought of as a coherent component plus a non-Rayleigh noise component. The behavior of these components may be predicted by the theory developed in this report.

VII. APPENDIX

VII.1 Calculation of $\rho_{rx}(\xi)$

$$\rho_{rx}(\xi) = \lim_{x\to\infty} \frac{\frac{1}{2x}\int_{-x}^{+x}\left[\cos(\Psi(x)) - \exp(-\frac{\Psi_o^2}{2})\right]\left[\cos(\Psi(x+\xi)) - \exp(-\frac{\Psi_o^2}{2})\right]dx}{\frac{1}{2x}\int_{-x}^{+x}\left[\cos(\Psi(x)) - \exp(-\frac{\Psi_o^2}{2})\right]^2 dx} \qquad (A.1)$$

Since Ψ is linearly related to surface height, its probability distribution $p(\Psi)$ is Gaussian.

$$p(\Psi) = \frac{1}{\sqrt{2\pi}\,\Psi_o} \exp\left(-\frac{\Psi^2}{2\Psi_o^2}\right)$$

The denominator of (A.1) represents an average which may just as well be found by averaging over Ψ instead of over x. Writing the denominator of (A.1) as an average over Ψ, we obtain:

$$\int_{-\infty}^{+\infty}\left[\cos(\Psi) - \exp(-\frac{\Psi_o^2}{2})\right]^2 p(\Psi)\,d\Psi = \frac{1}{2}\left[1 - \exp(-\Psi_o^2)\right]^2 \qquad (A.2)$$

Since Ψ is Gaussian its joint probability distribution in the x-direction $p_x(\Psi_1, \Psi_2)$, is given by

$$p_x(\Psi_1, \Psi_2) = \frac{1}{2\pi\,\Psi_o^2\sqrt{1-\rho_x^2(\xi)}} \exp\left\{\frac{-(\Psi_1^2 - 2\Psi_1\Psi_2\rho_x(\xi) + \Psi_2^2)}{2\Psi_o^2(1-\rho_x^2(\xi))}\right\}$$

where Ψ_1 and Ψ_2 are the phases of the field components contributed by two points on the surface separated by a distance ξ in the x-direction. Since the phase Ψ and the surface height are linearly

related, they have the same autocorrelation function. Thus $\rho_x(\xi)$ may be taken as the surface autocorrelation function in the x-direction. $p_x(\Psi_1, \Psi_2)$ is the probability distribution of Ψ_2 given Ψ_1 allowing for the proportion in which Ψ_1 itself occurs.

Like the denominator, the numerator of (A.1) represents an average which may be evaluated by averaging over Ψ. By using the joint probability distribution this average may be expressed as:

$$\int_{-\infty}^{+\infty} \int_{-\infty}^{+\infty} \left[\cos \Psi_1 \cos \Psi_2 - \cos \Psi_1 \exp\left(-\frac{\Psi_o^2}{2}\right) - \cos \Psi_2 \exp\left(-\frac{\Psi_o^2}{2}\right) + \exp\left(-\Psi_o^2\right)\right] p(\Psi_1, \Psi_2)\, d\Psi_1\, d\Psi_2 \qquad \text{(A.3)}$$

where Ψ_1 replaces $\Psi(x)$ and Ψ_2 replaces $\Psi(x + \xi)$.

Equation (A.3) may be integrated term by term. The first term is:

$$\frac{1}{2\pi \Psi_o^2 \sqrt{1 - \rho_x^2(\xi)}} \int_{-\infty}^{+\infty} \int_{-\infty}^{+\infty} \cos \Psi_1 \cos \Psi_2 \exp\left\{-\frac{\Psi_1^2 - 2\Psi_1 \Psi_2 \rho_x(\xi) + \Psi_2^2}{2\Psi_o^2 (1-\rho_x^2(\xi))}\right\} \cdot d\Psi_1\, d\Psi_2$$

By separating the numerator of the exponential term this expression becomes:

$$\frac{1}{K_1} \int_{-\infty}^{+\infty} \int_{-\infty}^{+\infty} \cos \Psi_1 \cos \Psi_2 \exp\left\{-\frac{-(\Psi_1 - \Psi_2 \rho_x(\xi))^2}{2K_2}\right\} \exp\left\{-\frac{\Psi_2^2}{2\Psi_o^2}\right\} d\Psi_1 d\Psi_2 \qquad \text{(A.4)}$$

where

$$K_1 = 2\pi \Psi_o^2 \sqrt{1 - \rho_x^2(\xi)}$$

$$K_2^2 = \Psi_o^2 \left(1 - \rho_x^2(\xi)\right)$$

The integral with respect to Ψ_1 is

$$\int_{-\infty}^{+\infty} \cos \Psi_1 \exp\left\{\frac{-(\Psi_1 - \Psi_2 \rho_x(\xi))^2}{2K_2^2}\right\} d\Psi_1 \ldots . \qquad (A.5)$$

making the substitution $a = (\Psi_1 - \Psi_2 \rho_x(\xi))$, we obtain

$$\int_{-\infty}^{+\infty} \cos (a + \Psi_2 \rho_x(\xi)) \exp\left(-\frac{a^2}{2K_2^2}\right) da = \sqrt{2\pi}\, K_2 \exp\left(-\frac{K_2^2}{2}\right) \cos \Psi_2 \rho_x(\xi) \ldots \qquad (A.6)$$

Substituting this result into (A. 4) and evaluating K_1 and K_2, we obtain

$$\frac{\exp\left\{-\frac{K_2^2}{2}\right\}}{\sqrt{2\pi}\,\Psi_o} \int_{-\infty}^{+\infty} \cos \Psi_2 \cos \Psi_2 \rho_x(\xi) \exp\left\{-\frac{\Psi_2^2}{2\Psi_o^2}\right\} d\Psi_2$$

since

$$\cos (A) \cos (B) = \frac{1}{2} \left(\cos (A - B) + \cos (A + B) \right)$$

the above expression integrates to

$$\exp\left\{-\Psi_o^2\right\} \cosh\left\{\Psi_o^2 \rho_x^2(\xi)\right\} . \ . \ . \qquad (A.7)$$

This is the first term of the integral (A. 3).

The second term of integral (A. 3) is

$$-\frac{\exp\left\{-\frac{\Psi_o^2}{2}\right\}}{K_1}\int_{-\infty}^{+\infty}\int_{-\infty}^{+\infty}\cos\Psi_1\exp\left\{\frac{-(\Psi_1-\Psi_2\rho_x(\xi))}{2K_2}\right\}\exp\left\{-\frac{\Psi_2^2}{2\Psi_o^2}\right\}$$

$$\cdot\, d\Psi_1\, d\Psi_2$$

The integral with respect to Ψ_1 is exactly equation (A. 5). Therefore, the above integral becomes

$$-\frac{\exp\left\{-\frac{\Psi_o^2}{2}\right\}\exp\left\{-\frac{K_2^2}{2}\right\}}{\sqrt{2\pi}\,\Psi_o}\int_{-\infty}^{+\infty}\cos(\Psi_2\rho_x(\xi))\exp\left\{-\frac{\Psi_2^2}{2\Psi_o^2}\right\}d\Psi_2$$

$$=\exp\left\{-\frac{\Psi_o^2}{2}\right\}\exp\left\{-\frac{K_2^2}{2}\right\}\exp\left\{-\frac{\Psi_o^2}{2}\rho_x^2(\xi)\right\}=-\exp\left\{-\Psi_o^2\right\}\quad\ldots\quad(A.8)$$

The third term of (A. 3) is also (A. 8) because $p(\Psi_1, \Psi_2)$ is symmetric with respect to Ψ_1 and Ψ_2. The fourth term of (A. 3) is

$$+\exp\left\{-\Psi_o^2\right\}:$$

because $\int_{-\infty}^{+\infty}\int_{-\infty}^{+\infty} p(\Psi_1, \Psi_2)\, d\Psi_1\, d\Psi_2$ is by definition 1.

Summing the terms of (A. 3) the numerator of (A. 1) is found to be

$$\exp\left\{-\Psi_o^2\right\}\cosh\left\{\Psi_o^2\rho_x(\xi)\right\}-1$$

Combining this with (A. 2), $\rho_{rx}(\xi)$ is

$$\rho_{rx}(\xi) = \frac{2 \exp\left\{ - \Psi_o^2 \right\} \cosh\left\{ \Psi_o^2 \rho_x(\xi) \ -1 \right\}}{\left[1 \ - \ \exp\left\{ - \Psi_o^2 \right\} \right]^2} \qquad \text{(A. 9)}$$

Ψ_o is the standard deviation of phase Ψ and $\rho_x(\xi)$ is the autocorrelation function of the surface in the x-direction.

$\rho_{ry}(\xi)$ is found by substituting y for x in the above argument. $\rho_{ry}(\xi)$ is thus

$$\rho_{ry}(\xi) = \frac{2 \exp\left\{1 - \Psi_o^2 \right\} \cosh\left\{ \Psi_o^2 \rho_y(\xi)) \ -1 \right\}}{\left[1 - \exp\left\{ - \Psi_o^2 \right\} \right]^2} \qquad \text{(A. 10)}$$

where $\rho_y(\xi)$ is the surface autocorrelation function in the y-direction.

The above expressions for ρ_{rx} and ρ_{ry} require only on the probability distribution of surface height of the scatterer be Gaussian.

VII. 2 Calculation of $\rho_{ix}(\xi)$

$$\rho_{ix}(\xi) = \lim_{x \to \infty} \frac{\frac{1}{2x} \int_{-x}^{+x} \sin\left\{ \Psi(x) \right\} \sin\left\{ \Psi(x+\xi) \right\} dx}{\frac{1}{2x} \int_{-x}^{+x} \left[\sin \left\{ \Psi(x) \right\} \right]^2 dx} \qquad \text{(A. 11)}$$

The numerator and denominator of equation (A. 11) represent averages which can be taken over Ψ just as well as over x. Again, assuming the Gaussian distribution of Ψ given by

$$p(\Psi) = \frac{1}{\sqrt{2\pi}\ \Psi_o} \quad \exp\left\{ - \frac{\Psi^2}{2 \Psi_o^2} \right\}$$

the denominator of equation (A.11) becomes

$$\int_{-\infty}^{+\infty} \sin^2 \Psi \, p(\Psi) \, d\Psi = \frac{1}{2}\left[1 - \exp\left\{-2\Psi_o^2\right\}\right] \qquad \text{(A.12)}$$

Applying the joint probability distribution of Ψ, $p_x(\Psi_1, \Psi_2)$, discussed in VII.1, the average in the numerator of (A.11) becomes:

$$\int_{-\infty}^{+\infty} \int_{-\infty}^{+\infty} \sin \Psi_1 \sin \Psi_2 \, p_x(\Psi_1, \Psi_2) \, d\Psi_1 \, d\Psi_2 \qquad \text{(A.13)}$$

As before, Ψ_1 corresponds to $\Psi(x)$ and Ψ_2 corresponds to $\Psi(x+\xi)$. Substituting $p_x(\Psi_1, \Psi_2)$ from VII.1, (A.13) becomes

$$\frac{1}{K_1} \int_{-\infty}^{+\infty} \int_{-\infty}^{+\infty} \sin\Psi_1 \sin\Psi_2 \exp\left\{-\frac{(\Psi_1 - 2\rho_x(\xi))^2}{2K_2^2}\right\} \exp\left\{-\frac{\Psi_2^2}{2\Psi_o^2}\right\} d\Psi_1 \, d\Psi_2 \qquad \text{(A.14)}$$

where

$$K_1 = 2\pi \Psi_o^2 \sqrt{1 - \rho_x^2(\xi)}$$

$$K_2^2 = \Psi_o^2 (1 - \rho_x^2(\xi))$$

The integral with respect to Ψ_1 is

$$\int_{-\infty}^{+\infty} \sin \left\{\Psi_1\right\} \exp\left\{-\frac{(\Psi_1 - \Psi_2 \rho_x(\xi))^2}{2K_2^2}\right\} d\Psi_1$$

Making the substitution $a = \Psi_1 - \Psi_2 \, \rho_x(\xi)$, we obtain

$$\int_{-\infty}^{+\infty} \sin\left\{a + \Psi_2 \rho_x(\xi)\right\} \exp\left\{-\frac{a^2}{2K_2^2}\right\} d\Psi_1 = \sqrt{2\pi}\, K_2 \sin\left\{\Psi_2 \rho_x(\xi)\right\} \exp\left\{-\frac{K_2^2}{2}\right\}$$

(A. 14) now becomes

$$\frac{\exp\left\{-\frac{K_2^2}{2}\right\}}{\sqrt{2\pi}\,\Psi_o} \int_{-\infty}^{+\infty} \sin\left\{\Psi_2\right\} \sin\left\{\Psi_2 \rho_x(\xi)\right\} \exp\left\{-\frac{\Psi_2^2}{2\Psi_o^2}\right\} d\Psi_2$$

since

$$\sin A \sin B = \frac{1}{2}\left[\cos(A - B) - \cos(A + B)\right]$$

The above integral becomes

$$\exp\left\{-\Psi_o^2\right\} \sinh\left\{\Psi_o^2 \rho_x(\xi)\right\} \qquad \text{(A. 15)}$$

Combining (A. 12) and (A. 15), $\rho_{ix}(\xi)$ becomes

$$\rho_{ix}(\xi) = \frac{2 \exp\left\{-\Psi_o^2\right\} \sinh\left\{\Psi_o^2 \rho_x(\xi)\right\}}{\left[1 - \exp\left\{-2\Psi_o^2\right\}\right]} \qquad \text{(A. 16)}$$

Ψ_o is the standard deviation of phase Ψ and $\rho_x(\xi)$ is the autocorrelation function of the surface in the x-direction.

$\rho_{iy}(\xi)$ is found by substituting y for x in the above argument, thus,

$$\rho_{iy}(\xi) = \frac{2 \exp(-\Psi_o^2) \sinh(\Psi_o^2 \rho_y(\xi))}{1 - \exp(-2\Psi_o^2)}$$

where $\rho_y(\xi)$ is the surface autocorrelation function in the y-direction.

The above expressions for ρ_{ix} and ρ_{iy} require only that the probability distribution of surface height of the scatterer be Gaussian.

VIII. REFERENCES

1. H. Davies, "The Reflection of Electromagnetic Waves from a Rough Surface," Proc. I.E.E., Monograph No. 90, 15 Jan. 1954.

2. C. I. Beard, "Coherent and Incoherent Scattering of Microwaves from the Ocean," I.R.E. Trans. on Antennas and Propagation, vol. AP-9, No. 5, September, 1961; pp. 470-483.

3. W. S. Ament, "Toward a Theory of Reflection by a Rough Surface," Proc. I.R.E., vol. 41, No. 1, January 1953; pp. 142-146.

4. R. H. Clarke, "Theoretical Characteristics of Radiation Reflected Obliquely from a Rough Conducting Surface," Proc. I.E.E., vol. 110, No. 1, January 1963; pp. 91-100.

5. R. F. Harrington, Time Harmonic Electromagnetic Fields, McGraw-Hill, New York, 1961 (Ch. 3, pp. 106-108).

6. S. Ramo and J. R. Whinnery, Fields and Waves in Modern Radio, John Wiley and Sons, New York, 2nd Ed., 1963 (Secs. 12.18 and 12.19, pp. 526-534).

7. F. Buckley and A. A. Nargott, "Tables of Dielectric Dispersion Data for Pure Liquids and Dilute Solutions," Circular 589, Natl. Bur. of Standards, 1958. (Superintendent of Documents, U. S. Government Printing Office, Washington, D. C.)

8. E. C. Jordan, Electromagnetic Waves and Radiating Systems, Prentice Hall, Englewood Cliffs, New Jersey, 1950(p. 116).

9. R. G. Manton, "The Reflection of Electromagnetic Waves from Rough Surfaces," Ph. D. Thesis, London University, 1958.

10. Chernov, Wave Propagation in a Random Medium, McGraw-Hill 1960 (pp. 6-11).